



OPEN Ecology and demographic structure of an extinct ibex population in late Upper Palaeolithic Italian Alps

Elena Armaroli^{1,10}✉, Francesco Fontani^{2,10}✉, Rocco Iacovera^{2,3}, Elisabetta Cilli², Adriana Latorre^{2,4}, Donata Luiselli², Sara Silvestrini², Gabriele Terlato², Giampaolo Dalmeri⁵, Alex Fontana⁵, Nicola Nannini⁵, Hubert Vonhof⁶, Lucio Calcagnile⁷, Gianluca Quarta⁷, Rossella Duches⁵, Eugenio Bortolini², Anna Cipriani^{1,8}, Stefano Benazzi², Federico Lugli^{1,9} & Matteo Romandini²✉

Alpine Upper Palaeolithic contexts exhibit specialised subsistence strategies, heavily dependent on *Capra ibex*. Among them, the rock shelter Riparo Dalmeri stands out, with *C. ibex* dominating faunal remains across all occupation phases, spanning the Pleistocene-Holocene transition. This evidence positions Riparo Dalmeri as a key site for exploring the interaction between human groups and *C. ibex* during this period of significant climatic and cultural shifts in human evolution. Here, we present the first multidisciplinary study on Late Palaeolithic *C. ibex* teeth from Riparo Dalmeri, integrating direct radiocarbon dating, stable isotope ($\delta^{13}\text{C}$, $\delta^{18}\text{O}$) and $^{87}\text{Sr}/^{86}\text{Sr}$ analyses, proteomic, and aDNA data. We generated the earliest aDNA sequences for *C. ibex* and contextual evidence on mobility, seasonality, and sex ratios. We found that most *C. ibex* were local to the area despite consistent human presence. They reveal significant dietary differences between sexes as well as increased seasonality at the Pleistocene-Holocene transition. Our results identify Riparo Dalmeri as belonging to an extinct branch of the ibex mtDNA phylogeny, offering unprecedented insights into ibex ecology and evolution that resonate with present-day issues on the conservation of this species in the face of climate change.

The Alpine ibex (*Capra ibex*) is undoubtedly a symbol of the Alps, with its presence attested since the Late Pleistocene¹. Nevertheless, human activities have long posed significant threats to its survival. Overhunting drove the Alpine ibex to near extinction in the early 19th century. The species was only able to recover recently, starting from a small population that survived in the Gran Paradiso National Park (Italy)². While the Alpine ibex is no longer considered an endangered species³, its natural habitat remains at risk, threatened by global warming^{4,5}. Recent DNA studies highlighted a complex population history for Alpine ibex in Europe, identifying major bottleneck events resulting from both environmental fluctuations and excessive human exploitation^{6,7}. These results importantly demonstrate the utility of ancient *C. ibex* genomic diversity and population size as proxies for reconstructing past ecological changes. In the Italian Alps, *C. ibex* played a key role in human subsistence since the Upper Palaeolithic, as testified by the widespread presence of remains in both valley floor and mid-altitude sites^{8–10}.

Among these sites, Riparo Dalmeri stands out as an exceptional case study. Located in the Northeastern Italian Alps (Trentino region) at 1240 m a.s.l., it was repeatedly occupied by Late Epigravettian hunter-gatherers focused on ibex hunting¹¹. Radiocarbon dating of charcoal and bone samples has identified three main phases of human occupation, spanning the critical climatic transition between the Pleistocene and the Holocene (13400

¹Department of Chemical and Geological Sciences, University of Modena and Reggio Emilia, via Campi 103, Modena 41125, Italy. ²Department of Cultural Heritage, University of Bologna, via degli Ariani 1, Ravenna 48121, Italy. ³Clinical Genetics Unit, Department of Women's and Children's Health, University of Padova, via Giustiniani 3, Padova 35128, Italy. ⁴Department of Biological, Geological and Environmental Sciences, via Selmi 3, Bologna 40126, Italy. ⁵MUSE, Science Museum, Corso del Lavoro e della Scienza 3, Trento 38123, Italy. ⁶Department of Climate Geochemistry, Max Planck Institute for Chemistry, Hahn-Meitner-Weg 1, Mainz 55128, Germany. ⁷CEDAD (Centre of Applied Physics, Dating and Diagnostics), Department of Mathematics and Physics "Ennio de Giorgi", University of Salento, via per Arnesano, Lecce 73100, Italy. ⁸Lamont-Doherty Earth Observatory, Columbia University, 61 Route 9W Palisades, New York, NY 10964, USA. ⁹Institut für Geowissenschaften, Goethe-Universität Frankfurt, Altenhöferallee 1, Frankfurt am Main 60438, Germany. ¹⁰Elena Armaroli and Francesco Fontani contributed equally to this work and share first authorship. ✉email: elena.armaroli@unimore.it; francesco.fontani2@unibo.it; matteo.romandini@unibo.it

– 11500 cal. BP¹²). Despite detailed studies of these three phases, significant uncertainties remain, particularly regarding human presence in the rock shelter during the Younger Dryas cold event (ca. 12900 – 11500 cal. BP¹³). These uncertainties are primarily due to the complex stratigraphy of the site^{12,14} (Supplementary Fig. S1). Riparo Dalmeri can be defined as a specialised ibex-hunting site¹⁵, with *C. ibex* remains representing 80%–93% of identified species across all three phases of occupation (Supplementary Data 1). While ibex represents an important component of faunal assemblages at other contemporaneous sites in northern Italy⁸, the consistently high proportion documented at Riparo Dalmeri are exceptional, making it a key context for understanding human-ibex relationships during a period of climatic transition.

Here, we address Late Pleistocene *C. ibex* ecology and evolution through a multidisciplinary study on ibex teeth recovered within the entire stratigraphic sequence of Riparo Dalmeri. Six new direct radiocarbon dates were obtained to refine our understanding of human occupation of the site at the end of the Upper Palaeolithic. Strontium (⁸⁷Sr/⁸⁶Sr), carbon ($\delta^{13}\text{C}$) and oxygen ($\delta^{18}\text{O}$) isotope analyses are used to provide a detailed picture of *C. ibex* diet and mobility, and to reconstruct the paleoclimate of this transitional period in the Italian Alps. Ancient DNA data – coupled with proteomic analysis of tooth enamel – are used to determine the sex of individuals. We also explore the genetic population structure of Riparo Dalmeri ibex and its relationship to other ancient and modern ibex populations. Our findings are discussed considering (1) the complex relationship between the hunter-gatherers of Riparo Dalmeri and their favourite prey and (2) the implications of this multi-proxy study for understanding the challenges faced by Alpine ibex in the current period of climate change.

Results

Revisiting the stratigraphic succession at Riparo Dalmeri

The zooarchaeological material analysed in this study was selected to secure an even representation of the three identified phases of human occupation at the site (Table 1). New radiocarbon dates (Supplementary Data 2) confirm the higher intensity of human activities during Phase 1 (13550 – 12950 cal. BP, 1 σ) and Phase 2 (12950 – 12600 cal. BP, 1 σ), corresponding to the first part of the Younger Dryas. The new dates from the upper layers of Phase 3 (13100 – 11450 cal. BP, 1 σ) support its integrity and coherence with the Pleistocene-Holocene transition and Younger Dryas, despite a partial overlap with the previous phases due to a plateau in the calibration curve around 12400 cal. BP (Fig. 1). Although trampling and other post-depositional processes may have caused some vertical and horizontal displacement of anthropogenic material, the overall integrity of the stratigraphic deposit is supported by field observations, lithic refittings, and the coherent spatial distribution of the findings.

Paleoclimate reconstruction and the Alpine ibex ecology

The local comparative samples ⁸⁷Sr/⁸⁶Sr range between 0.70816 and 0.70834 (mean = 0.70822, SD = 0.00015; $n = 4$). Tooth enamel ⁸⁷Sr/⁸⁶Sr values of the whole dataset span between 0.70794 and 0.70886 (mean = 0.70817, SD = 0.00021; $n = 26$) (Fig. 2a), with no significant variations across different age classes, sexes, or occupation phases of the site. The calculated Tukey interquartile range ($k = 1.5$) of ibex enamel samples spans from 0.70761 to 0.70863. Ibex teeth from the first phase display values between 0.70796 and 0.70825, with a mean of 0.70812 (SD = 0.00012; $n = 4$). ⁸⁷Sr/⁸⁶Sr values from the second occupation phase range between 0.70794 and 0.70886, with a mean of 0.70817 (SD = 0.00024; $n = 14$, including four different tooth classes from the same individual). Samples from the third phase of occupation yielded a mean of 0.70818 (SD = 0.00022; $n = 8$), ranging between 0.70794 and 0.70859. Based on local comparative samples and the Tukey IQR, only the most radiogenic sample, RD_8203 (⁸⁷Sr/⁸⁶Sr = 0.70886; second phase), can be considered an outlier. The majority (twenty-five out of twenty-six) of ⁸⁷Sr/⁸⁶Sr values fall within the local range defined by the baseline and the local Sr isoscape around the site^{16–18} (Fig. 3). Thus, ibex teeth from Riparo Dalmeri can be considered a reliable paleoclimatic proxy for studying the local environment through $\delta^{13}\text{C}$ and $\delta^{18}\text{O}$ isotope analysis of hydroxyapatite carbonate-moiety.

Sequential C and O stable isotope analysis of eighteen selected ibex teeth ($n = 243$ data points) yielded $\delta^{13}\text{C}_{\text{VPDB}}$ values ranging from -12.2 to -9.8‰ (mean = -10.9‰), with no significant intra-tooth variation ($\sim 1\text{‰}$; Figs. 2b and 4). Overall, these $\delta^{13}\text{C}$ values are typical of C_3 plant feeders¹⁹, consistent with Western European vegetation patterns²⁰. No remarkable differences were observed among occupation phases (mean = -11.1 , -10.9 and -10.8‰ , respectively; Fig. 2c). A significant difference (Wilcoxon rank-sum test $p < 0.01$) between females and males suggests dietary or habitat-related differences between sexes (Fig. 2d). The $\delta^{18}\text{O}_{\text{VPDB}}$ values range between -8.5‰ and -2.2‰ (mean = -6‰) with high intra-tooth variation (up to 6.2‰ , sample RD_8158; Figs. 2b and 4), suggesting seasonal fluctuations in the local environment²¹. No significant difference between sexes was observed (Wilcoxon rank-sum test $p = 0.42$).

Overall, the variability observed in enamel $\delta^{18}\text{O}$ data (recalculated as ingested water) matches the modern predicted monthly precipitation $\delta^{18}\text{O}$ time-series from Pistoia²² (Fig. 5) at the coordinates of Riparo Dalmeri. Given the known ibex tooth formation time²³ and the observed seasonal $\delta^{18}\text{O}$ peaks, individual teeth likely capture between six to twelve months of life history. The mean $\delta^{18}\text{O}$ values are similar among the three occupation phases, indicating overall colder conditions than today (Fig. 6). Interestingly, the signal amplitude is significantly higher in the third phase. Air temperature estimates from oxygen isotopes suggest summer temperatures reach their highest ($\sim 30\text{ °C}$) in summer and their lowest ($\sim -5\text{ °C}$) in winter in this phase. A statistically significant correlation between $\delta^{18}\text{O}$ and $\delta^{13}\text{C}$ values was observed in six out of eighteen samples ($p < 0.05$), with four showing negative correlations and two positive correlations (Fig. 7).

Sample ID	SU	Phase	Species	Tooth class	Age class
RD_8189	26d	1	<i>C. ibex</i>	M3	Adult I
RD_8190	26d	1	<i>C. ibex</i>	M3	Adult II
RD_8191	26d	1	<i>C. ibex</i>	M3	Adult I
RD_8192	26d	1	<i>C. ibex</i>	M3	Adult II
RD_8193	26d	1	<i>C. ibex</i>	M3	Adult I
RD_8194	26d	1	<i>C. ibex</i>	M3	Adult II
RD_8195	26d	1	<i>C. ibex</i>	M3	Adult II
RD_8198	26e	1	<i>C. ibex</i>	M3	Young Adult
RD_8179	26b	2	<i>C. ibex</i>	M3	Adult II
RD_8184	26b roof	2	<i>C. ibex</i>	M3	Adult I
RD_8185	26b roof	2	<i>C. ibex</i>	M3	Adult I
RD_8202	26c	2	<i>C. ibex</i>	M3	Adult II
RD_8203	26c roof	2	<i>C. ibex</i>	M3	Adult II
RD_8204	26c roof	2	<i>C. ibex</i>	M3	Adult II
RD_8205	14b	2	<i>C. ibex</i>	p2	Young adult
RD_8206	14b	2	<i>C. ibex</i>	p3	Young adult
RD_8210a	14b	2	<i>C. ibex</i>	p3	Young
RD_8210b	14b	2	<i>C. ibex</i>	p4	Young
RD_8210c	14b	2	<i>C. ibex</i>	M1	Young
RD_8210d	14b	2	<i>C. ibex</i>	M2 gem	Young
RD_8215	14	2	<i>C. ibex</i>	p4	Young
RD_8218	26c	2	<i>C. ibex</i>	p4	Young
RD_8156	77	3	<i>C. ibex</i>	M3	Young adult
RD_8158	64	3	<i>C. ibex</i>	M3	Adult I
RD_8159	77	3	<i>C. ibex</i>	M3	Senile
RD_8161	77	3	<i>C. ibex</i>	M3	Adult II
RD_8163	78	3	<i>C. ibex</i>	M3	Adult I
RD_8168	21	3	<i>C. ibex</i>	M3	Young adult
RD_8173	26 cleaning	3	<i>C. ibex</i>	M3	Young adult
RD_8175	26	3	<i>C. ibex</i>	M3	Young adult
RD_8177	26	3	<i>C. ibex</i>	M3	Young adult
RD_8219	26	na	Micromammal	Incisor	na
RD_8220a	26	na	Micromammal	Incisor	na
RD_8224	26	na	Micromammal	Incisor	na
RD_8230	78	na	<i>Lepus timidus</i>	Incisor	na

Table 1. Zooarchaeological material from Riparo Dalmeri.

The Dalmeri ibex mitochondrial phylogeny

Genetic data were generated from twelve well preserved teeth from Riparo Dalmeri. Additional samples were collected from the prehistoric sites of Riparo Cogola (NE Italy, $n = 2$) and Romagnano Loc III (NE Italy, $n = 2$) to provide a broader picture of genomic variability in Late Pleistocene Alpine ibex (Fig. 8a).

The samples reported 0.213% to 43.06% of preserved endogenous DNA when mapped to the nuclear reference genome of *Capra hircus* (ARS1.2). For each individual the total number of unique reads mapped to the Alpine ibex reference mitogenome (NC_020623.1) was consistently greater compared to mapping statistics to the mitochondrial references of other species of the *Capra* genus. Given the low coverage nature of the data (from 0.2x to 0.0003x), nuclear genomes were only used to assess the sex of the individuals. Analysis of degradation confirms authenticity of aDNA (Fig. 8b). We reconstructed mitogenomic information from eleven of the twelve samples of Riparo Dalmeri, with mean coverages ranging 2x to 40x. Only samples with mean coverage $\geq 9x$ were included in the main phylogenetic analysis ($n = 6$). All samples from Riparo Cogola and Romagnano Loc III, which had lower coverage, were analysed separately in a dataset of low-quality mitogenomes. The Maximum Likelihood (ML) tree computed from a dataset of modern and ancient *Capra* species (“*Capra_all*”) shows that *C. ibex* and *C. pyrenaica* cluster together, forming a well-supported monophyletic clade for the European wild ibex (Figs. 8c and 9) that is distinct from the remaining goat species from Eurasia and North East Africa, as well as from the domestic goat (*C. hircus*). Within this clade, Riparo Dalmeri forms a sub-clade with sister group *C. pyrenaica*, while all historic *C. ibex* samples are located between Riparo Dalmeri and modern samples.

The Bayesian phylogeny (Fig. 10a) supports the same tip topology and the same monophyletic origin of the Pyrenean specimens, with estimated divergence time between *C. ibex* and *C. pyrenaica* at 43500 – 31600 years BP (95% Highest Posterior Density, HPD). All modern *C. ibex* samples cluster together ($p = 0.91$), including the

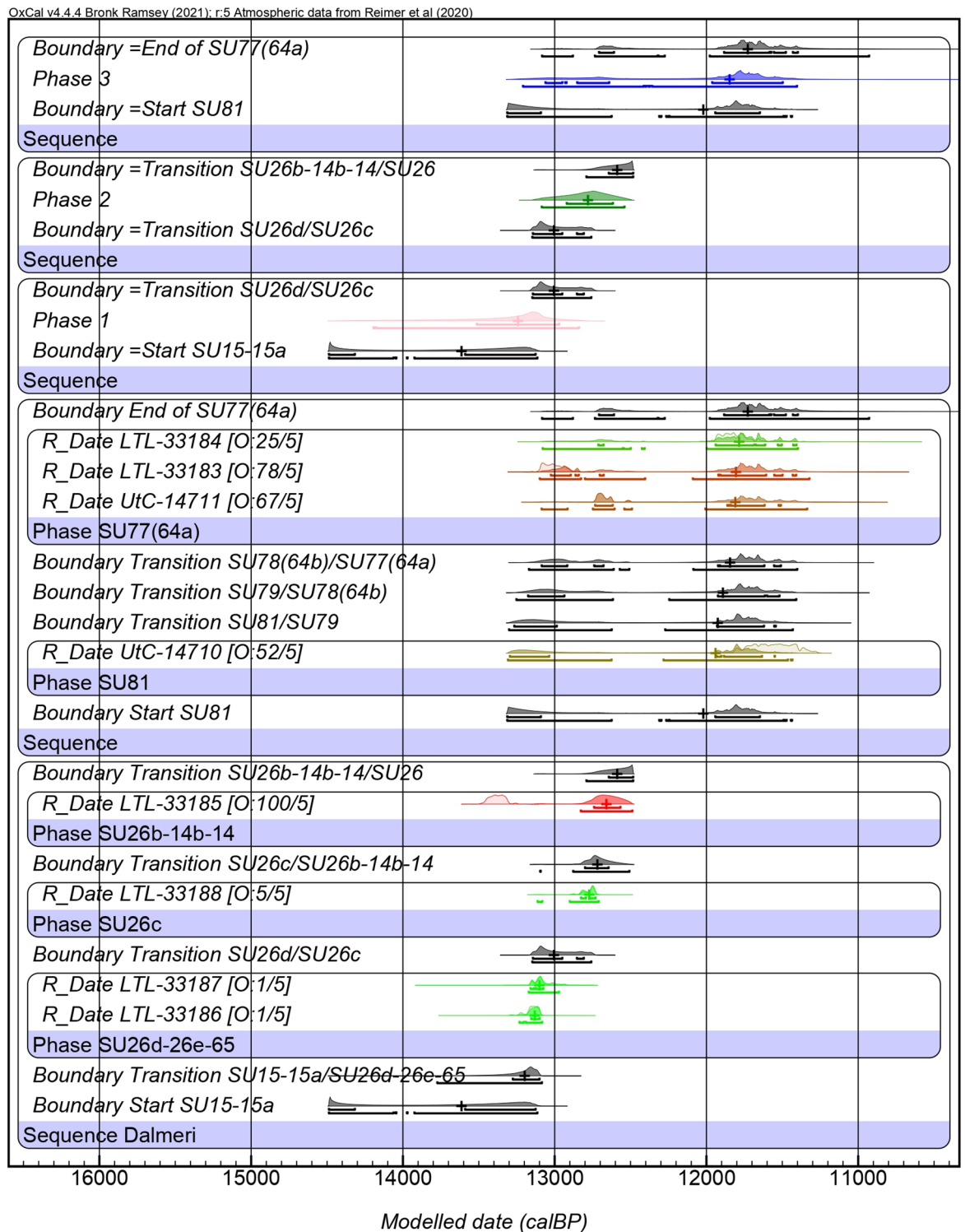


Fig. 1. Bayesian modelled ^{14}C dates from Riparo Dalmeri inner (1–2) and outer (3) frequentation phases calculated after direct radiocarbon analysis of bones and teeth samples.

historic Swiss (Zu01 and Be4) and Italian Gran Paradiso samples. Riparo Dalmeri segregates from other ancient samples, including the geographically closest Ötzi_stomach ($P=0.73$), with an estimated divergence time of 41100–29800 years BP (95% HPD).

The same topology is further supported by our mtDNA network (Fig. 10b), which displays a total of twenty-six distinct haplotypes divided into five haplogroups. Among them, haplogroup A only contains the ancient samples from Riparo Dalmeri, and the other ancient samples are segregated from modern and historic samples into distinct haplogroups. The Bayesian skyline shows that the population size did not experience significant

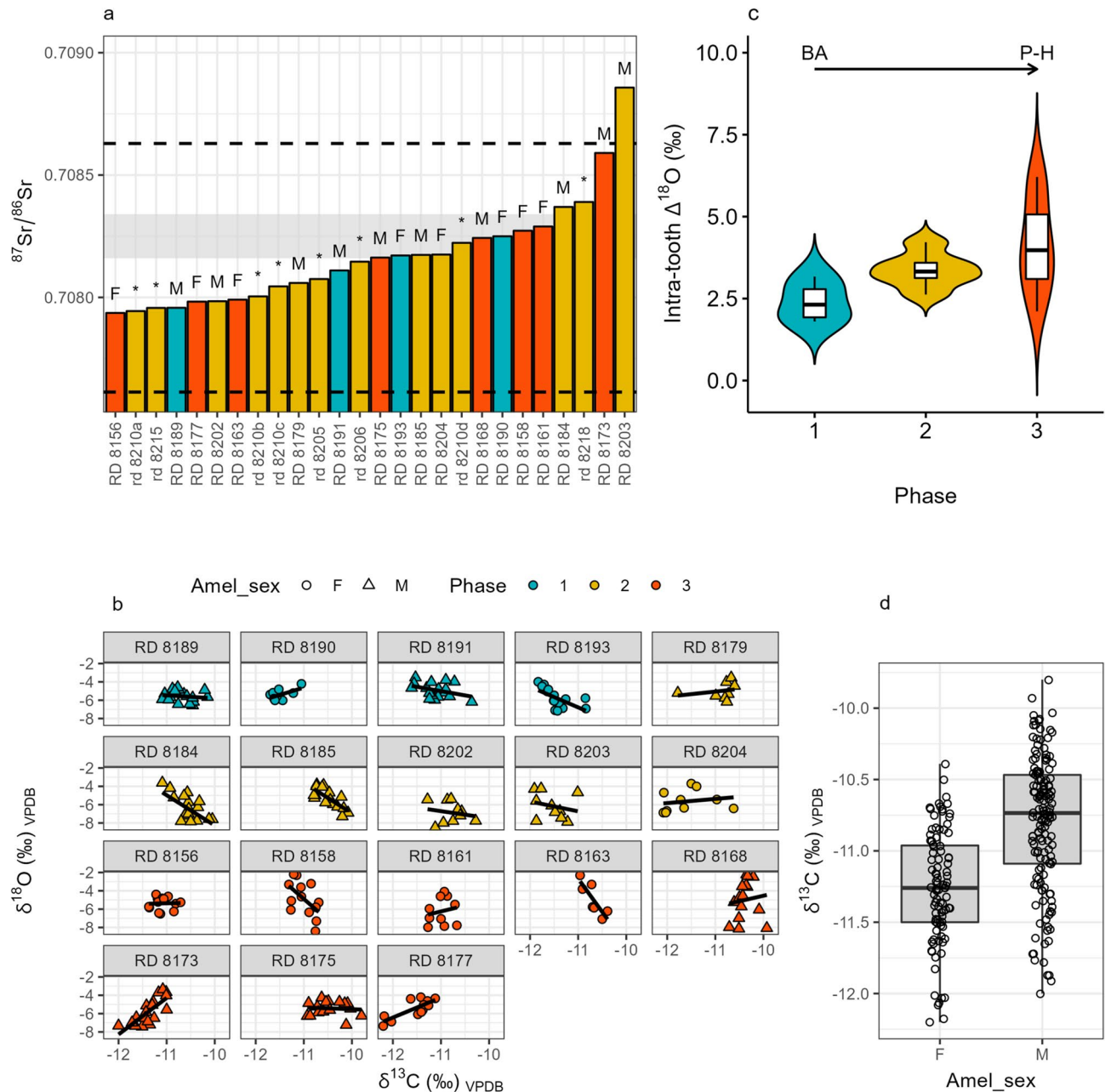


Fig. 2. (a) $^{87}\text{Sr}/^{86}\text{Sr}$ ratios for each individual (sex is labelled as “M” = male and “F” = female; “*” = deciduous tooth); the grey area represents the measured local comparative samples (i.e., $n = 3$ micromammal and $n = 1$ hare teeth; max-min); the dashed lines represent the Tukey IQR ($k = 1.5$) of ibex samples; the Italian isoscape indicates a much larger range for the local Sr isotope signature at Dalmeri (between ~ 0.708 and ~ 0.711 at 10 km radius), possibly including the whole dataset of *C. ibex*; (b) Intra-tooth $\delta^{18}\text{O}$ vs. $\delta^{13}\text{C}$ values for each individual, coloured by phase (light blue = 1, yellow = 2, orange = 3), with symbols representing sexes (circles = female, triangle = male); (c) Calculated intra-tooth $\Delta^{18}\text{O}$ variability (max-min) for each individual, clustered by phase of site occupation, between the Bølling–Allerød (BA) interstadial and Pleistocene–Holocene (P–H) transitional period; (d) $\delta^{13}\text{C}$ values by ibex sex (Wilcoxon rank-sum test $p < 0.01$).

fluctuations during the Late Pleistocene (Fig. 11). Conversely, a visible population decline coincides with the large-scale growth of human populations in historic times. Notably, these results are consistent with the pairwise comparison analysis; the average genetic distances within Riparo Dalmeri (haplogroup A = 0.135) and the other ancient samples (haplogroup B = 0.127, and haplogroup C = 0.091) are approximately three times greater than that of the modern and historical samples in haplogroup D (0.044) and E (0.014). However, the average genetic distances in haplogroup A compared to haplogroups B and C are only 0.008% and 0.043% greater, respectively. Pairwise distances among ancient samples (Table 2) show consistently higher dissimilarity between Riparo Dalmeri and other ancient samples.

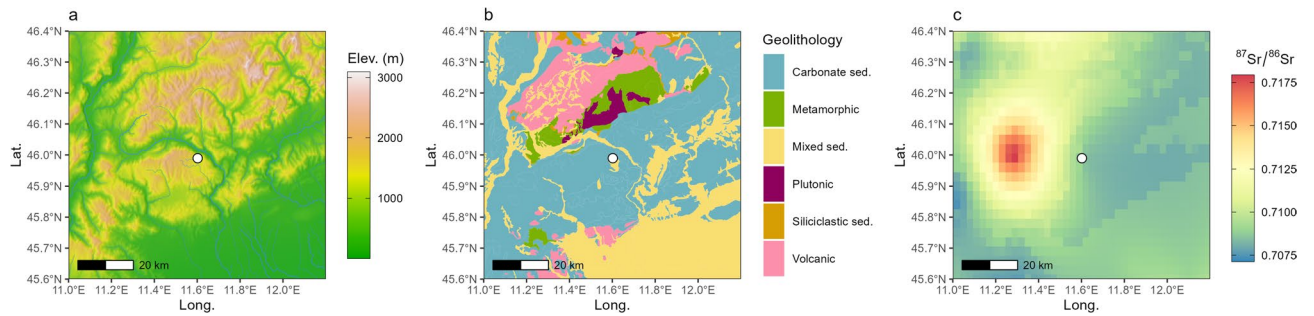


Fig. 3. (a) Digital elevation model of the area surrounding Riparo Dalmeri (white circle), obtained from the `get_elev_raster` R function (<https://github.com/USEPA/elevatr>), which utilises the Amazon Web Services (<https://registry.opendata.aws/terrain-tiles/>) terrain tiles and the Open Topography Global Datasets API; rivers are from Lehner and Grill¹⁷; (b) Simplified geological map from GLiM¹⁸; (c) Local Sr isotope around the site from Lugli et al.¹⁶.

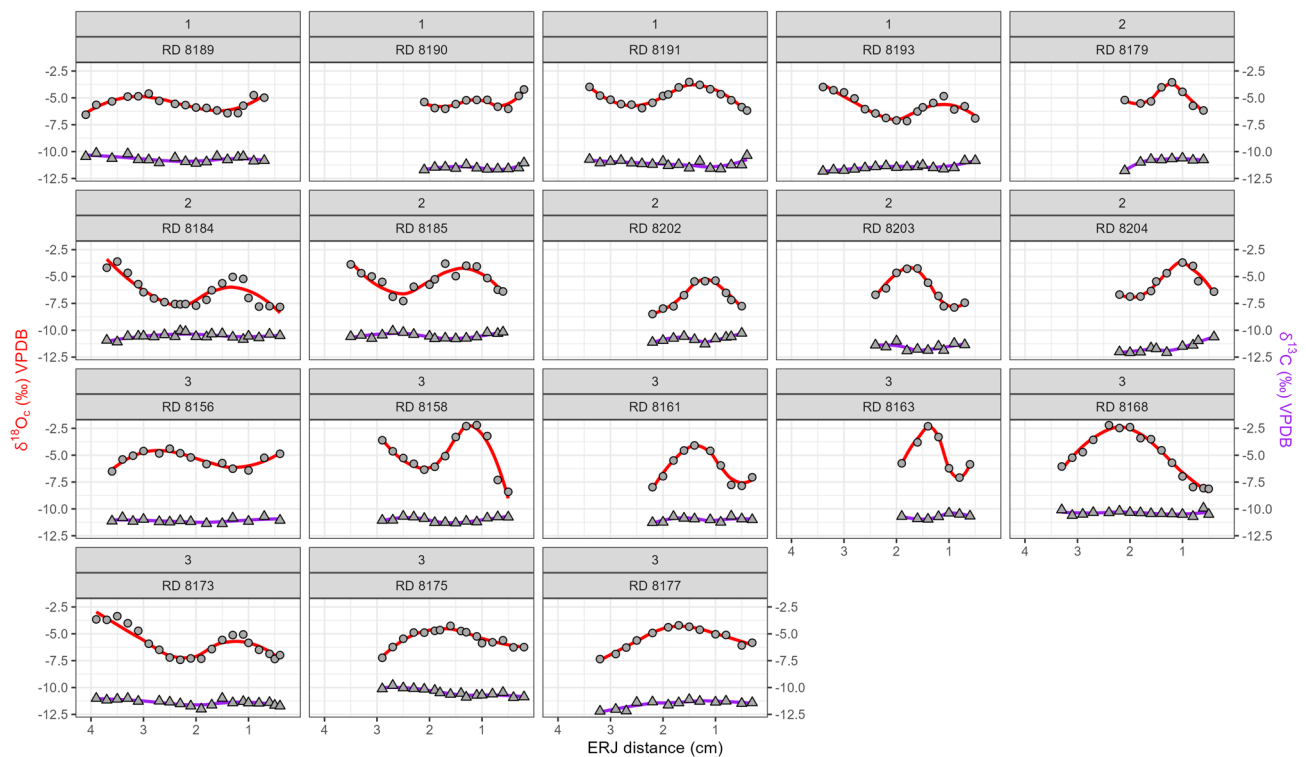


Fig. 4. Intra-tooth $\delta^{18}\text{O}$ and $\delta^{13}\text{C}$ (‰ VPDB) profiles. Carbon isotope values (triangles, purple profiles) are homogeneous within samples, while oxygen isotope values (circles, red profiles) show sinusoidal patterns indicative of local climate fluctuations.

A combined approach for sex assignment in prehistoric Alpine ibex

Proteomic sex estimation was performed exploiting the sex-specificity of AMELX and AMELY protein isoforms encapsulated in tooth enamel. The presence of both unique AMELX and AMELY peptides in fifteen fossil samples indicates male individuals, while the remaining eight samples, in which only AMELX peptides were observed, are likely female. The detailed procedure is described in the Supplementary Text.

Sex was also identified in ten of the eleven specimens sequenced for ancient DNA. Even at extremely low coverage (mean < 0.0003), DNA-based determination with both the Rx and Ry values matched five out of six results obtained by amelogenin analysis on overlapping samples. Overall, genetic results unambiguously identified six male and four female individuals. Due to low coverage, RD_8158 reported borderline results on both Rx (0.734, CI 0.687–0.782) and Ry (0.026, CI 0.023–0.029) estimates. However, amelogenin analysis, along with an extremely low quantity of DNA sequences mapping to Y-chromosome regions ($n = 313$), suggests the individual was female. Read depth statistics for Y-chromosome, X-chromosome, and autosomal regions further support the consistency of the methods.

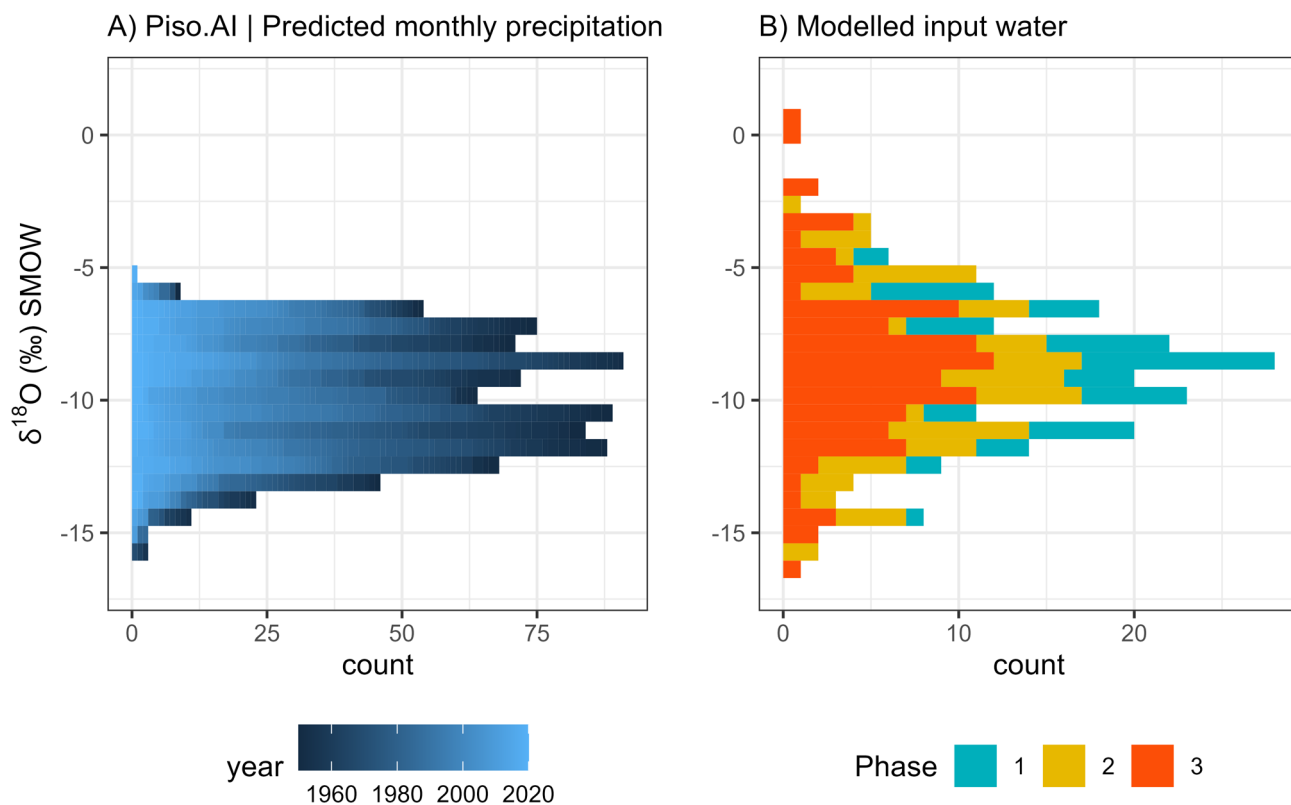


Fig. 5. Comparison of (a) modern predicted monthly time-series precipitation $\delta^{18}\text{O}$ at the coordinates of Riparo Dalmeri (Piso.AI; <https://isotope.bot.unibas.ch/PisoAI/>) with (b) modelled data $\delta^{18}\text{O}$ (input water) from ibex teeth. In (a) data from the last 70 years were reported.

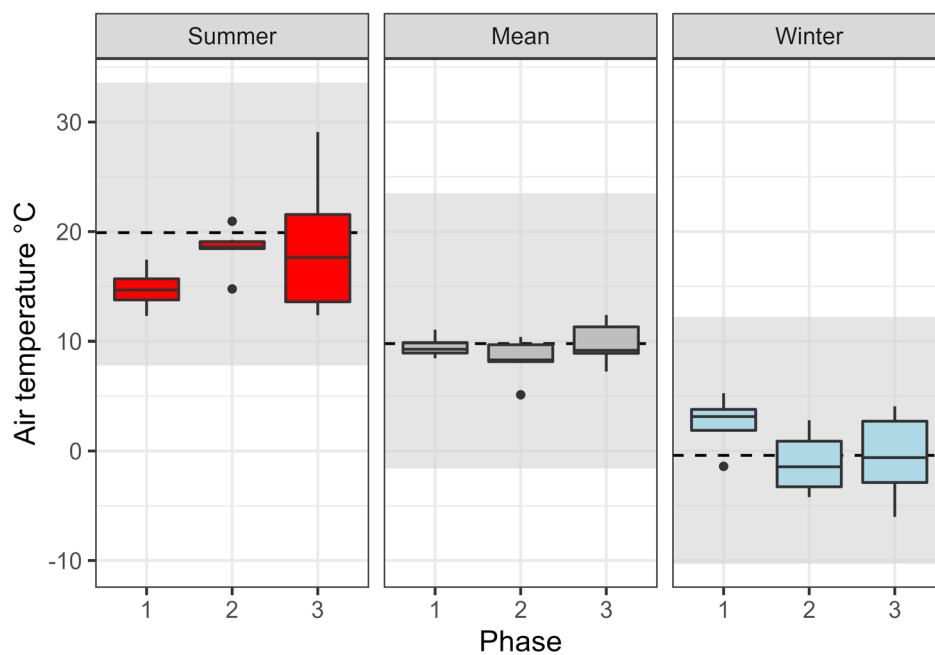


Fig. 6. Summer, mean, and winter air temperature estimation divided by phase, obtained from modelled input water oxygen isotope data of ibex enamel. The dashed lines represent the mean temperature for summer, winter, and year time range in Borgo Valsugana (TN). Gray areas are the maximum-minimum ranges.

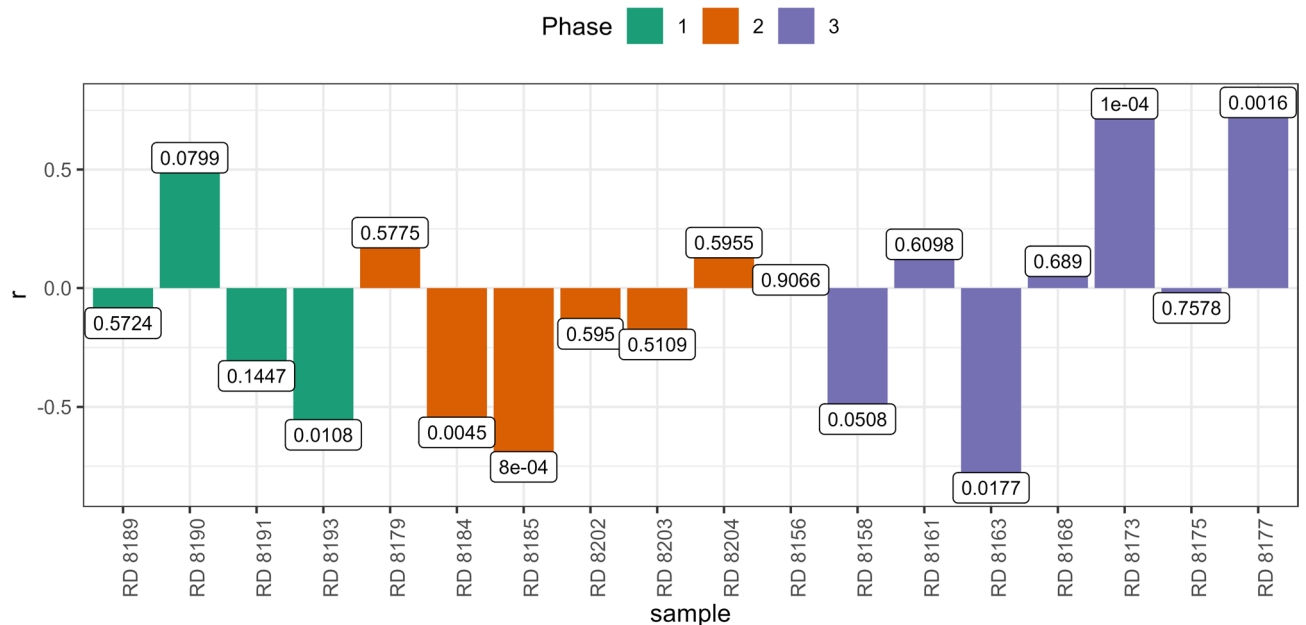


Fig. 7. Linear correlation between $\delta^{18}\text{O}$ and $\delta^{13}\text{C}$ values of ibex teeth ($n = 18$) divided by site occupation phase. The correlation coefficient $r > 0.5$ indicates a strong positive correlation (i.e., C-O covariation), while $r < 0.5$ indicates a strong negative correlation (i.e., C-O anti-covariation). Labels are p-values.

Discussion

Previous research has suggested that Riparo Dalmeri was a seasonal site specialised in ibex hunting²⁴, a camp site where all family members – including children^{25,26} – lived seasonally, basing most of their subsistence on ibex^{15,27}. The abundance of *C. ibex* remains and the recurrent presence or representation of this species in dwelling structures, hearths, ornaments, and portable art, make Riparo Dalmeri a unique case study in the entire European continent for studying the interaction between this taxon and humans on the verge of a pivotal climatic and cultural tipping point.

In this work, new direct radiocarbon dates, together with literature data, confirm that Riparo Dalmeri was frequented during the Late Glacial, primarily during the Bølling-Allerød interstadial (13550–12950 cal. BP, 1 σ ; first phase), when Late Epigravettian hunter-gatherers began to recolonise the mountains. Despite the presence of reworked materials, the new dates (12950–11450 cal. BP, 1 σ ; second and third phases) suggest anthropic frequentation, and thus ibex hunting, also during the Younger Dryas or Pleistocene-Holocene transition. This is supported by the presence of lithic tools coherent with this chronological period).

We also explored the genetic footprint of Riparo Dalmeri ibex to provide a new understanding of its population structure in light of the extensive pressure posed by specialised hunting activities. Our findings confirm previous evidence on the mitochondrial phylogenetic relationships among different *Capra* species. Here, *Capra ibex* forms a distinct monophyletic clade. Based on radiocarbon dates and Bayesian phylogeny, we now estimate that the divergence between *Capra ibex* and *Capra pyrenaica* occurred ~ 37550 years BP, post-dating previous estimates by nearly 10000 years⁶. In the Bayesian tree, the Riparo Dalmeri ibex population forms a distinct branch, possibly representing an ancestral, geographically isolated, and extinct population within the ibex mtDNA phylogeny. This structure may have consolidated during the Last Glacial Maximum, when ice coverage reached its peak, extending over large parts of Northern Europe and the Alps²⁸. When compared with samples from the coeval and geographically close sites of Riparo Cogola and Romagnano Loc III, Riparo Dalmeri still emerges as a genetically segregated population. It should be noted, however, that the very low coverage of the former yields unreliable results. This limitation hampers statistical support and warrants caution in interpretation; for this reason, these results are not discussed further. On the other hand, the geographic and temporal distance of Riparo Dalmeri from the other high-coverage ancient samples analysed in this study may explain at least part of their genetic segregation. This genetic model will benefit from the future inclusion of additional ancient sequences from both sides of the Alpine range.

As far as population size over time is concerned, the Riparo Dalmeri population shows levels of haplotype and nucleotide diversity consistent with other ancient samples, suggesting a stable density of *Capra ibex* during the Late Pleistocene, despite intensive hunting and consistent human presence. Despite a rise in temperatures and consequent changes in Alpine habitats, as well as increasing human activity²⁹, our analysis does not show a decrease in population size after the LGM. A drastic decline in intraspecific genetic diversity can only be detected between the 16th and 18th centuries due to increased anthropogenic pressure on the ecosystem, followed by a dramatic bottleneck which almost drove the species to extinction after the 18th century^{7,30}.

Proteomic and isotope analyses carried out in this study shed light on the ecology of this extinct and isolated population in the broader context of the marked climatic variability characterising the end of the Late Glacial

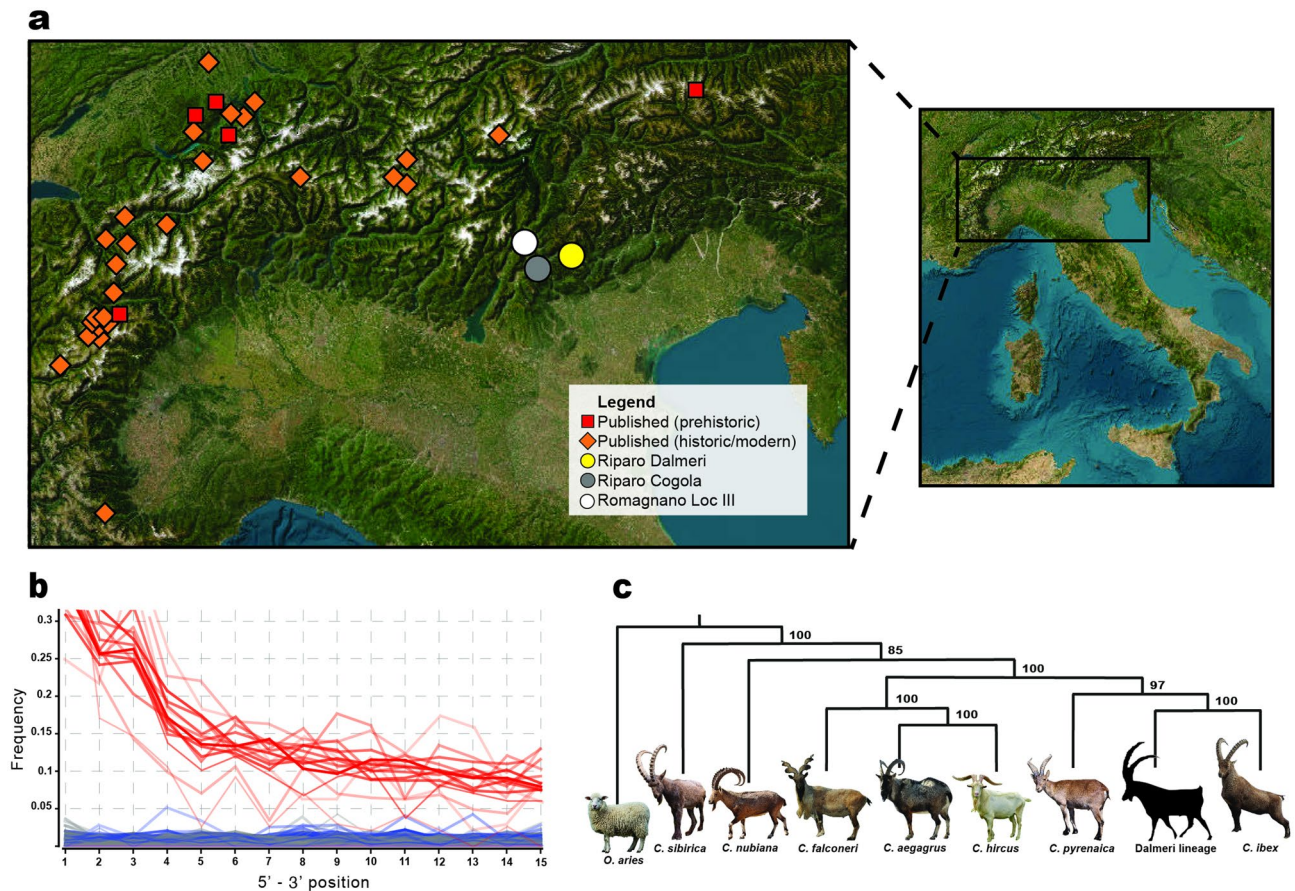


Fig. 8. (a) Geographic origin of the published and new ibex genetic data analysed in this study. Esri, World Topographic Map. Map was edited in Adobe Illustrator CC 2020; (b) Recurrence of damage patterns in the form of C > T transitions (red lines) at 5' end positions of single-stranded DNA sequences for newly generated mitogenomes. Blurred lines are used for samples with mean coverage < 5x; (c) A simplified Maximum Likelihood tree summarises the phylogenetic history of *Capra* species, with samples from Riparo Dalmeri clustering in the branch of *Capra ibex*. *Ovis aries* is used as the outgroup.

period. Here, for the first time, we compare amelogenin and aDNA results on sex determination in ancient animal samples. We identified eight females out of twenty-three samples, indicating that both sexes of different age classes were present around the site during human occupation of the shelter, likely coinciding with the ibex hunting season^{24,31}. Ecological studies suggest that modern ibex primarily move seasonally through altitudinal shifts over relatively short distances (from 6 to 22 km)³². Even shorter distances have been observed in the autochthonous population of Gran Paradiso National Park, showing a degree of fidelity to seasonal home ranges³³. The low variability of our ⁸⁷Sr/⁸⁶Sr values, which align with the local baseline, supports the idea of limited seasonal movements³⁴. Considering the low degree of modern ibex mobility and the significant variability of ⁸⁷Sr/⁸⁶Sr values in the area¹⁶ (Fig. 3), the two samples identified as possible outliers (RD_8203; RD_8173) likely reflect short-range mobility. Notably, both outliers are males. Modern studies show that present-day male and female ibex select different habitats throughout the year, with males using larger home ranges^{1,35,36}.

The relatively high $\delta^{13}\text{C}$ values in the Dalmeri samples are typical of semi-open environments³⁷ and are consistent with recently published $\delta^{13}\text{C}$ values from ibex bone collagen (SU 26b – c)³⁸. Small intra-tooth variations could result from the narrow isotopic range documented in C_3 -dominated environments of temperate and boreal ecosystems³⁹, but might also reflect the limited mobility indicated by Sr isotopes. The lack of significant differences across the three occupation phases (mean values $\sim -11\text{‰}$) may be related to these factors.

However, we cannot exclude that the $\sim 1\text{‰}$ intra-tooth variation reflects altitudinal mobility. A decrease in ^{13}C discrimination with altitude has been extensively documented in C_3 plants^{40,41} and various animal species, suggesting potential altitudinal shifts of about 200 metres³⁹. Altitudinal mobility is also often indicated by a negative correlation between $\delta^{13}\text{C}$ and $\delta^{18}\text{O}$ values in tissues of animals living in mountain environments^{42,43}. However, in our dataset, 12 out of 18 ibex samples do not show a significant correlation between these two values ($p > 0.05$; Fig. 7). Sex-related differences in altitude use do not appear to explain these variations. Among the six samples that show a significant correlation ($p < 0.05$), both sexes are represented, which is consistent with previous studies suggesting no major sex differences in altitude use³⁴. Conversely, a significant $\delta^{13}\text{C}$ difference between sexes in fossil *C. ibex* individuals (Fig. 2d) aligns with ecological data on modern ibex. The strong

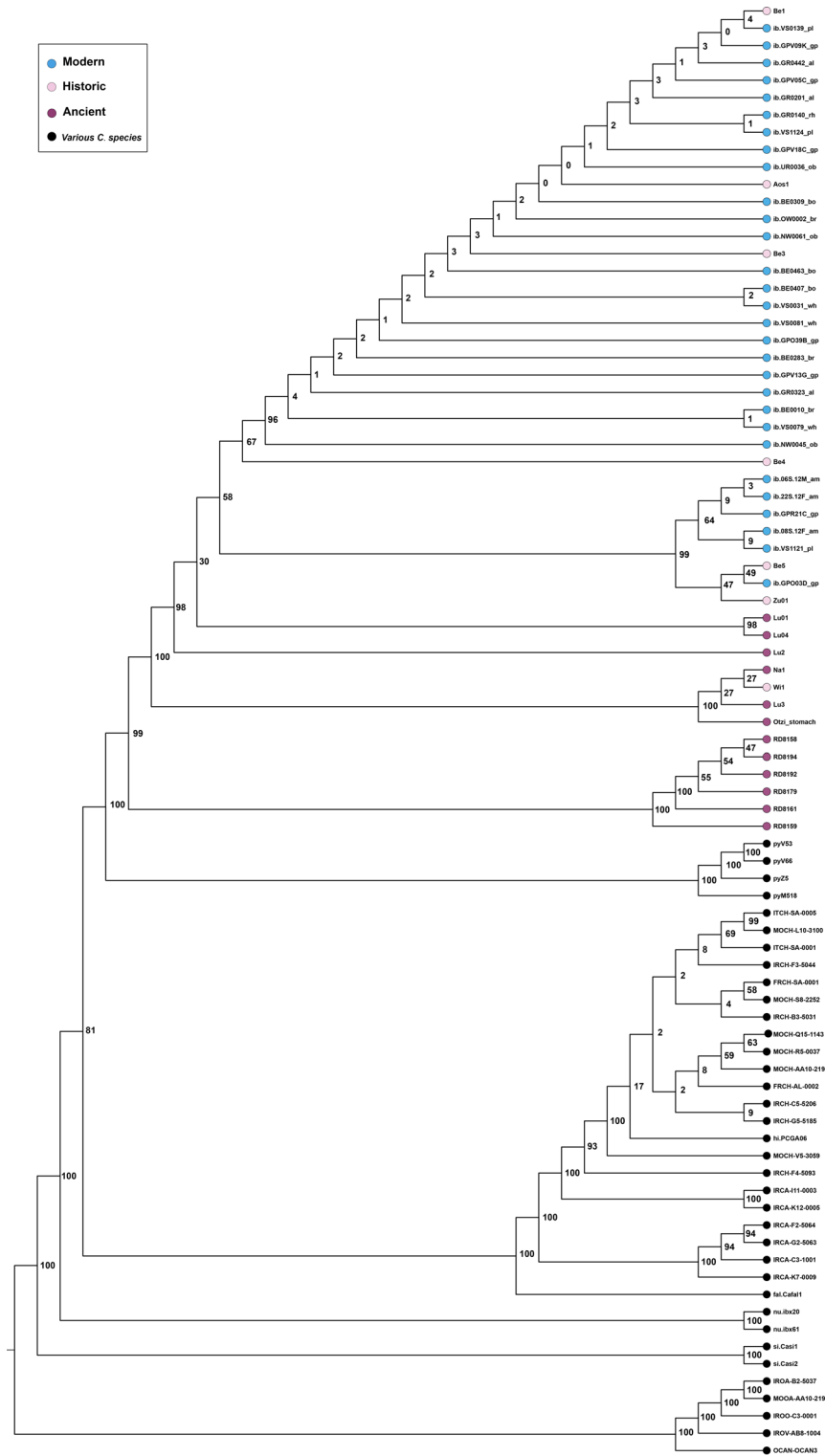


Fig. 9. Maximum likelihood tree with high-coverage samples.

sexual dimorphism, along with other factors like pregnancy and the presence of ibex offspring, leads to habitat segregation and distinct plant consumption patterns for much of the year^{35,44}.

From an environmental perspective, oxygen isotopes provide key insights into the paleoclimate at Riparo Dalmeri. Because ibexes are obligate drinkers⁴⁵, their $\delta^{18}\text{O}$ values mainly reflect local water sources, which are closely linked to local environmental parameters⁴⁶. Lower values correspond to winter and higher values to summer months²¹. All ibex samples show a clear sinusoidal pattern in their $\delta^{18}\text{O}$ values, indicating seasonal changes in the local environment (Fig. 4), with no notable differences between males and females. Interestingly,

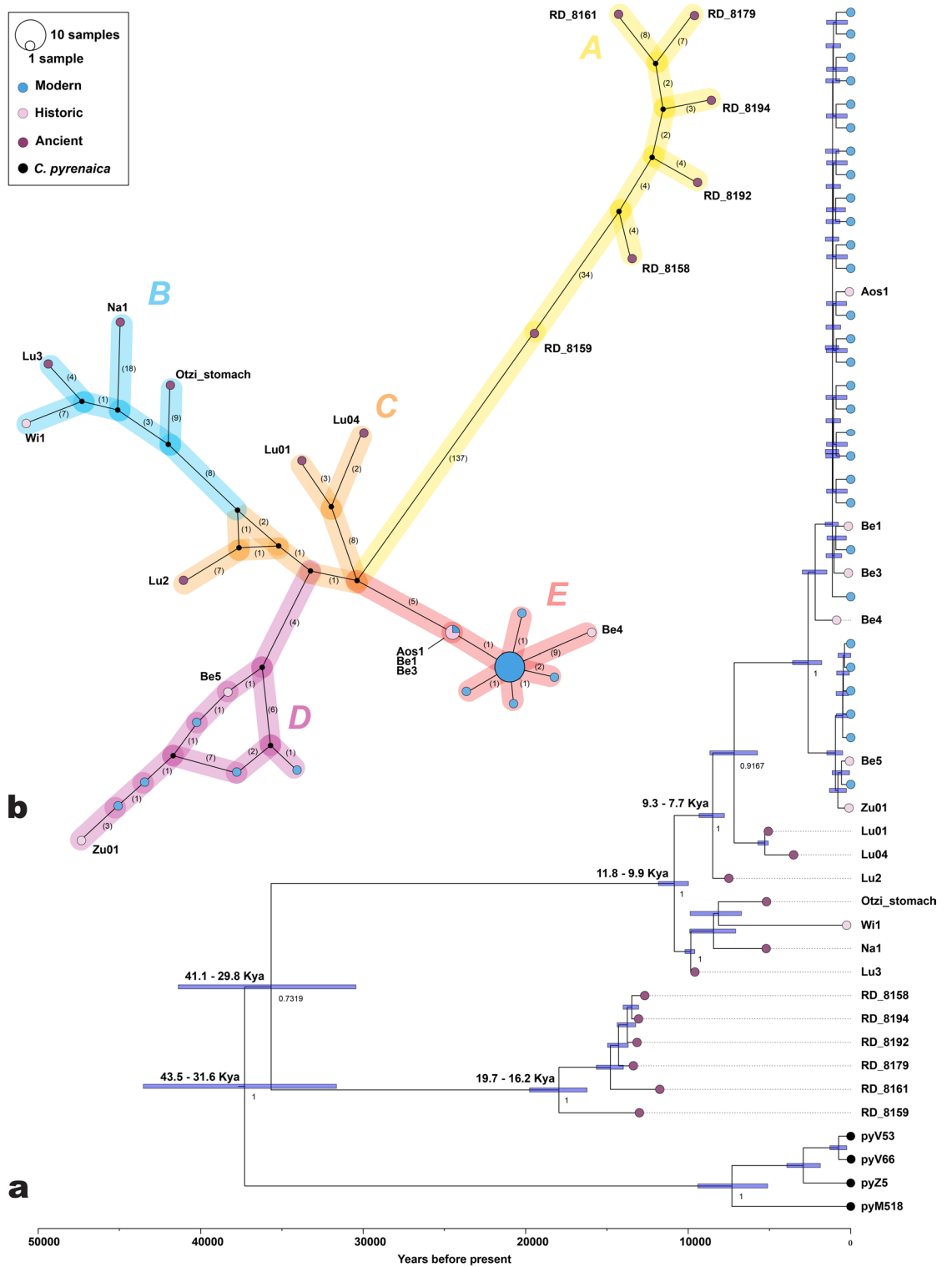


Fig. 10. (a) The Bayesian tree constructed using the “Capra_ibex/pyrenaica” dataset. Branch labels denote the posterior probabilities, and node labels indicate inferred split times. All key parameters exhibited effective sample sizes (ESS) exceeding 200, indicating that the MCMC chains were well-mixed and stabilised. The light blue blocks surrounding the nodes represent the 95% HPD intervals. Branch tips for *Capra ibex* are colour-coded: blue for modern samples, pink for historical samples, and purple for ancient samples. Black branch tips represent samples of *Capra pyrenaica*. (b) Haplotype network of the mtDNA sequences from the dataset “Capra_ibex”. A single substitution step is represented by a single number connecting two haplotypes. Non-sampled intermediary haplotypes are represented by black vertices connecting two or more haplotypes. The chronological context of the samples can be identified by their colours, as indicated in the legend.

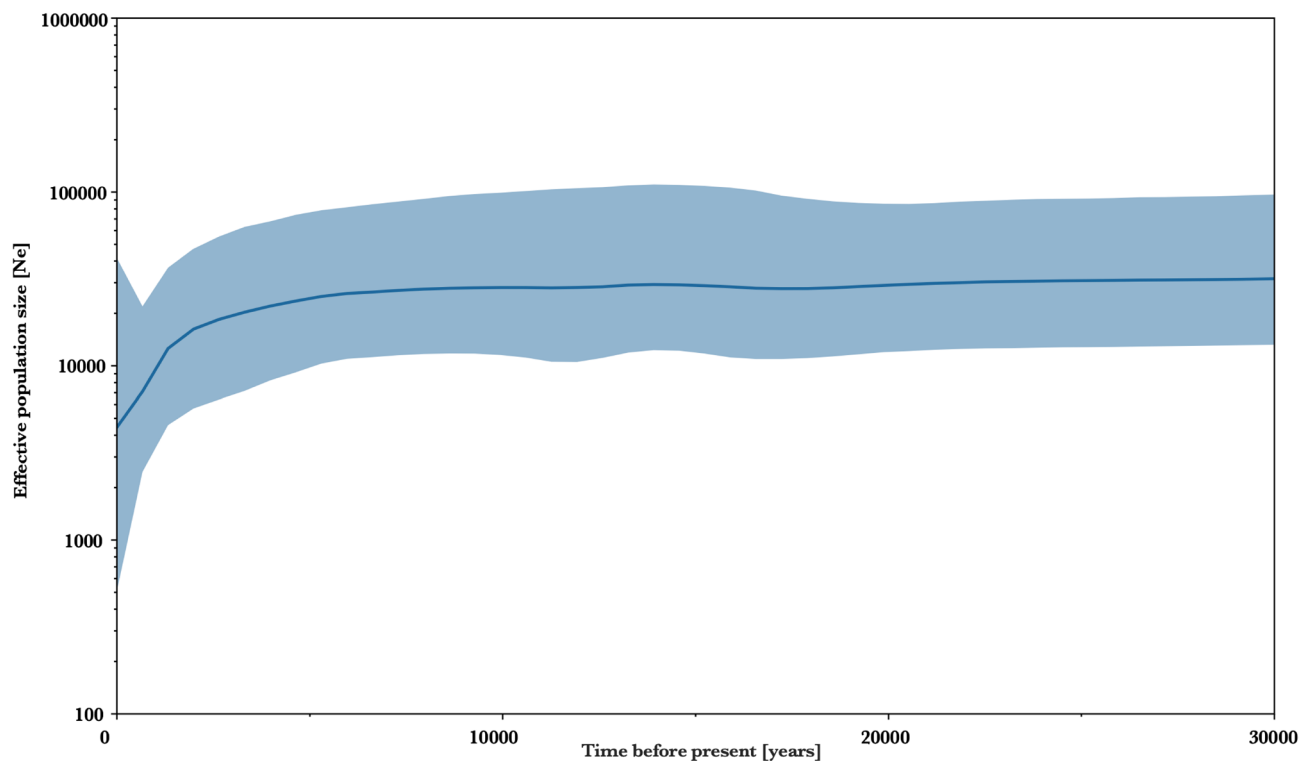


Fig. 11. Bayesian skyline plot based on the *Capra ibex* dataset. A mutation rate of 2.73×10^{-7} under a strict clock model was used, with an MCMC chain of 25 million samples. The x-axis represents time, while the y-axis represents the population size of *Capra ibex* expressed as N_e .

	Lu3	Na1	Ötzi	Lu01	LuD4	Lu2	RD8158	RD8159	RD8161	RD8179	RD8192	RD8194
Lu3												
Na1	0,0014											
Ötzi	0,0010	0,0018										
Lu01	0,0016	0,0024	0,0022									
Lu04	0,0016	0,0022	0,0019	0,0054								
Lu2	0,0014	0,0023	0,0019	0,0013	0,0010							
RD8158	0,0105	0,0112	0,0105	0,0109	0,0106	0,0106						
RD8159	0,0090	0,0096	0,0091	0,0091	0,0088	0,0088	0,0023					
RD8161	0,0108	0,0115	0,0109	0,0114	0,0111	0,0111	0,0010	0,0051				
RD8179	0,0107	0,0113	0,0108	0,0111	0,0108	0,0108	0,0011	0,0023	0,0009			
RD8192	0,0110	0,0117	0,0111	0,0115	0,0112	0,0112	0,0007	0,0024	0,0008	0,0008		
RD8194	0,0111	0,0118	0,0112	0,0117	0,0114	0,0114	0,0008	0,0026	0,0008	0,0007	0,0005	

Table 2. Pairwise distance for all high-coverage ancient *Capra ibex* samples.

most samples from the third phase exhibit a larger amplitude (‰) of $\delta^{18}\text{O}$ values (Fig. 6). This increased amplitude suggests that the environment underwent more pronounced seasonal changes during this period compared to the Bølling-Allerød interstadial. These findings seem to reflect the climatic shifts associated with the onset of the Younger Dryas and the subsequent Pleistocene-Holocene transition. Estimated air temperatures further support this interpretation. In the third phase, the highest temperature reached $\sim 30^\circ\text{C}$ and the lowest temperatures dropped to $\sim -5^\circ\text{C}$, mirroring modern seasonal temperature fluctuations recorded at the meteorological station of Borgo Valsugana ($\sim 400\text{ m a.s.l.}$, 25 km from Riparo Dalmeri; Fig. 6). We are aware that uncertainties in the model and the stratigraphy of the third occupation phase, especially for samples from the external succession, do not allow us to draw firm conclusions. However, several studies have reported that the Younger Dryas in the northern hemisphere was characterised by cool, dry winters and shorter summers than the Bølling-Allerød interstadial, even though summer temperatures were comparably high^{47,48}. Our isotope data are consistent with this pattern.

These environmental and ecological findings complement our genetic insights. While our isotope data revealed increased seasonality in the environment during the third phase, likely linked to the onset of the Younger Dryas and the Pleistocene-Holocene transition, the genetic data suggest that such environmental pressures, along with intensified human hunting, might have driven shifts in ibex ecology. Changes in ibex “seasonality” and habitat use due to changes in climatic conditions have been widely documented^{1,33,34,36}. As the climate changed, the ibex population of Riparo Dalmeri likely adjusted their seasonal home ranges, which in turn could have influenced patterns of human activity at the site. Therefore, the archaeological evidence of sporadic human frequentations at the end of the Epigravettian could be related to a decreased availability of their favourite prey. Later, during the Holocene, ibex became restricted to high mountain refuges⁴⁹, an occurrence echoed today in the Alpine region in response to heat stress⁵⁰. The simultaneous action of anthropic pressure and the sudden change in the environment may have left the ibex population of Riparo Dalmeri insufficient time to adapt, leading to its extinction.

Together, the genetic, isotopic and archaeological evidence paints a coherent picture of how climatic shifts, human activities, and geographical isolation shaped the evolutionary history and population dynamics of extinct *Capra ibex* at Riparo Dalmeri. We believe that this type of analysis should be more frequently integrated into archaeological and palaeoecological research, as it can help address critical issues such as the conservation and management of animal species threatened by human-induced climate change.

Methods

Material selection and archaeozoological analysis

A detailed description of the archaeological contexts considered in this study is provided in the Supplementary Text. Osteological samples from all the sites involved in the study were provided by the MUSE – Science Museum of the autonomous province of Trento (Italy).

Both adults ($n = 22$) and young individuals’ teeth ($n = 8$) were selected. Since they are easier to recognise and more suitable for intra-tooth sequential sampling, only permanent third molars were selected for adult individuals. For young individuals, both permanent molars and deciduous premolars were selected. Age classes were determined following Fiore and Tagliacozzo²⁷. The determination of the minimum number of individuals (MNI) for each occupation phase was performed to avoid sampling teeth from the same individual. The MNI count was carried out considering both the side (i.e., left or right) and the tooth wear^{23,51}. Moreover, the maximum anterior-posterior diameter (MAP) and the transversal diameter (TD) were measured on third molars only to allow comparison with the dimensions of ibex teeth from other Italian Palaeolithic sites (Supplementary Tables S1 and S2; Supplementary Figs. S2 and S3).

To build the local ⁸⁷Sr/⁸⁶Sr baseline, plant and water samples could not be collected due to the current inaccessibility of the site. Therefore, we analysed archaeological fauna found during excavations at Riparo Dalmeri and provided by the MUSE (see Holt et al.⁵² for a review). These samples consisted of $n = 1$ *Lepus timidus* tooth enamel and $n = 3$ undetermined micromammal tooth enamel. Detailed information about the samples is provided in Table 1. To identify potential outliers, the Tukey interquartile range limits were calculated for the ibex samples as $Q1 - k * IQR$ (lower bound) and $Q3 + k * IQR$ (upper bound), with $k = 1.5$.

Radiocarbon dating

Collagen was extracted from $n = 6$ ibex samples by using the Longin protocol⁵³ at the chemical laboratories of the Centre for Applied Physics, Dating and Diagnostics (CEDAD) Department of Mathematics and Physics “Ennio de Giorgi” University of Salento⁵⁴. A fraction of the collagen extracted was used for the determination of the C:N ratio (EA-Mod. Flash 2000 HT by Thermo). All the measured C:N ratios fall within range considered optimal (2.9–3.6), indicating the good preservation of the analysed collagen. The fraction selected for ¹⁴C analysis was combusted to CO₂ in sealed quartz tubes with CuO and Silver wool and then reduced at 600 °C to graphite with H₂ on Fe powder used as catalyst. AMS ¹⁴C measurements were carried out with the 3 MV Tandem at CEDAD-University of Salento (High Voltage Engineering Europa BV Mod. as in Calcagnile et al.⁵⁵. The measured ¹⁴C/¹²C isotopic ratios were corrected for isotopic fractionation by using the $\delta^{13}C$ term measured on line with the accelerator, and for machine and chemical processing background. The conventional ¹⁴C ages were then calculated according to Stuiver and Polach⁵⁶ and calibrated by using the last internationally accepted IntCal20⁵⁷ calibration curve. Data (Supplementary Data 2) were analysed and phase duration was inferred through a contiguous stratigraphic Bayesian model for Phases 1 and 2 and an overlapping/independent sequence for the external Phase 3, both using a uniform prior, in OxCal v4.4.4^{58–60} on the stratigraphic sequence published in Angelucci et al.¹². The Zenodo link to the original code needed to reproduce the model is provided in the Data Availability section.

Isotope analyses

Isotope analyses were carried out on dental enamel of $n = 18$ permanent ibex teeth from all three phases of occupation of the site, and $n = 8$ deciduous ibex teeth. ⁸⁷Sr/⁸⁶Sr isotope analysis was performed on both adult and young ibex individuals, as well as on 4 baseline samples. Sample preparation and Sr separation were carried out at the MeGic laboratory of the Department of Chemical and Geological Sciences of the University of Modena and Reggio Emilia. About 5–10 mg of each sample (‘bulk’) was dissolved in 3M HNO₃. Strontium was separated from the matrix using chromatographic Teflon columns filled with 30 μ l of Eichrom Sr spec resin⁶¹. The resin was cleaned with MilliQ water and conditioned using 3M HNO₃ before sample loading. Cations (not Sr) were desorbed by percolating 3M HNO₃. Sr was then eluted with several reservoirs of MilliQ water. The sample solutions obtained were diluted using 4% HNO₃, and the ⁸⁷Sr/⁸⁶Sr isotopic compositions were measured using a Thermo Fisher Neptune MC-ICPMS, housed at the Centro Interdipartimentale Grandi Strumenti of the University of Modena and Reggio Emilia, as described in Lugli et al.^{62,63}. Mass bias normalisation was performed

through exponential law using an $^{88}\text{Sr}/^{86}\text{Sr}$ ratio of 8.375209⁶⁴. Repeated analysis of NBS-SRM987 yielded an $^{87}\text{Sr}/^{86}\text{Sr}$ ratio of 0.710213 ± 0.000018 (2SD, $n = 14$). Samples were reported to an accepted NIST-SRM987 value of 0.710248⁶⁵. Tooth enamel from the 18 adult specimens was sequentially sampled for oxygen ($\delta^{18}\text{O}$) and carbon ($\delta^{13}\text{C}$) isotope analysis. Samples ~ 0.1 cm wide were drilled ~ 0.2 cm apart, starting from the occlusal surface (older enamel) to the enamel-root junction (younger enamel), overall corresponding to ~ 1 year of life²³. Depending on the tooth length and wear, we were able to obtain between 7 and 20 enamel samples per tooth. The analysis on the carbonate moiety of enamel hydroxyapatite was carried out at the inorganic stable isotope laboratory of the Department of Climate Geochemistry at the Max Planck Institute for Chemistry in Mainz. About 200–400 μg of enamel powder per sample was analysed on a Thermo Delta V mass spectrometer equipped with a GASBENCH-II preparation device. Within a run of 40 samples, a total of 11 replicates of two in-house tooth enamel standards (AG-Lox, MAMMY) were analysed. Standard materials were selected to cover the full range of sample weights. The AG-Lox tooth enamel standard has a $\delta^{13}\text{C}$ value of -11.58‰ and a $\delta^{18}\text{O}$ value of -1.42‰ , and the tooth enamel standard MAMMY has a $\delta^{13}\text{C}$ value of -13.49‰ and a $\delta^{18}\text{O}$ value of -14.76‰ . Following correction for size effects, AG-Lox typically shows a reproducibility better than 0.1‰ (1SD) for $\delta^{13}\text{C}$ and 0.16‰ (1SD) for $\delta^{18}\text{O}$. MAMMY serves as a control standard, exhibiting comparable $\delta^{13}\text{C}$ reproducibility to AG-Lox, while $\delta^{18}\text{O}$ values display slightly higher variability, with an uncertainty of less than 0.25‰ at the 1SD level. All data were reported to the VPDB (Vienna Pee Dee Belemnite) scale⁶⁶. The complete list of isotopic results is available in Supplementary Data 3.

Inverse modelling and paleotemperature reconstruction

Due to the long time required for tooth mineralisation and the sampling procedures, time-averaging and amplitude-damping effects occur between the measured intra-tooth isotope values and the actual isotopic variations recorded in the enamel during tooth formation. Therefore, before using the intra-tooth $\delta^{18}\text{O}$ values for seasonal paleotemperature estimation, inverse modelling was applied to recover the environmental input signal^{67,68}. We are aware that this model was developed for continuously growing teeth, yet no specific model exists for med-sized bovids such as ibex (see Kohn⁶⁹ and cf. Pederzani et al.^{70,71}).

The initial mineral content of enamel was set at 25%, enamel appositional length at 10 mm, and maturation length at 13 mm (see Zazzo et al.⁷²). During the modelling workflow, a damping factor describing the damping of the isotopic profile amplitude needs to be iteratively chosen using an adjustment of the measured error term (E_{meas}) to the prediction error (E_{pred}). The adjusted damping factors used here ranged between 0.01 and 0.03. Carbonate $\delta^{18}\text{O}$ values were converted to phosphate ($\delta^{18}\text{O}_{\text{ph}}$)⁷³ and then to $\delta^{18}\text{O}$ of ingested water ($\delta^{18}\text{O}_{\text{w}}$) using the formula for *Capra* sp. from Delgado-Huertas et al.⁷⁴. The modelled input $\delta^{18}\text{O}$ profiles are shown in Fig. 12. Summer, winter, and mean air temperature estimation were obtained for all three occupation phases and compared with modern air temperature from Borgo Valsugana (TN; Fig. 6). To convert water values ($\delta^{18}\text{O}_{\text{w}}$) into air temperature data we used the linear regression for Europe from⁷⁵. To generate summer and winter estimates, highest and lowest values from the inverse model for each tooth were used as input values for the temperature conversion. Mean annual temperatures were calculated averaging all the inverse modelling estimations.

Amelogenin analysis: sex estimation

Ibex sex was assessed on $n = 23$ adult specimens through the identification of amelogenins (AMELX and AMELY) in tooth enamel. The method was set up and tested on $n = 3$ modern *Capra ibex* with known sex (two males and one female) from the Gran Paradiso National Park, part of the Bones Lab archaeozoological collection. Sample preparation and protein extraction were performed at the Bones Lab of the Department of Cultural Heritage in Ravenna (UNIBO) and at the Department of Chemical and Geological Sciences (UNIMORE). For each individual, about 100 mg of enamel was sampled using a dentist drill. After rinsing with MilliQ water in an ultrasonic bath, the enamel chunks were leached for 5 min in 200 μL of 5% HCl and washed again with MilliQ. Samples were left overnight at room temperature in 750 μL of 1.2M HCl to extract enamel proteins. The solution was then collected and refrigerated. Enamel chunks were soaked again in 750 μL of 1.2M HCl and left overnight at room temperature. The two HCl solutions were then combined, and the peptides were extracted and purified using C_{18} in-house stage tips following the protocol for faunal samples described in Cappellini et al.⁷⁶. Samples were finally measured by an LC-MS/MS, housed at the Centro Interdipartimentale Grandi Strumenti of the University of Modena and Reggio Emilia, using a Dionex Ultimate 3000 UHPLC coupled to a high-resolution Q Exactive mass spectrometer (Thermo Scientific, Bremen, Germany) (as in Lugli et al.⁷⁷). A Top5 DDA mode was selected with no inclusion list. Raw data were searched against a FASTA reference dataset generated ad-hoc, including dental proteome sequences from UniProt, using both Mascot and MaxQuant (Supplementary Figs. S4 and S5). Enzymatic digestion was set to 'unspecific' and the following variable modifications were included: oxidation (M), deamidation (NQ), and phosphorylation (ST). The final sex estimation, based on bovine reference sequences (entries AMELX_BOVIN P02817 and AMELY_BOVIN Q99004), is a combination of the results from the two searches (Supplementary Table S3). The detailed proteomic data analysis is described in the Supplementary Text, including the estimates of deamidation and peptide lengths (Supplementary Figs. S6 and S7).

Ancient DNA workflow

A total of $n = 4$ teeth for each phase of the Riparo Dalmeri rock shelter were selected for the genetics analysis, along with additional samples from Riparo Cogola ($n = 2$) and Romagnano Loc III ($n = 2$) to provide a broader baseline for the genetic variability of prehistoric ibex in the Alpine range. The ancient DNA workflow was conducted in the ancient facilities of the Department of Cultural Heritage (University of Bologna). The aDNA laboratory is physically separated from other laboratories of the institute and is pressurised to reduce air-influx,

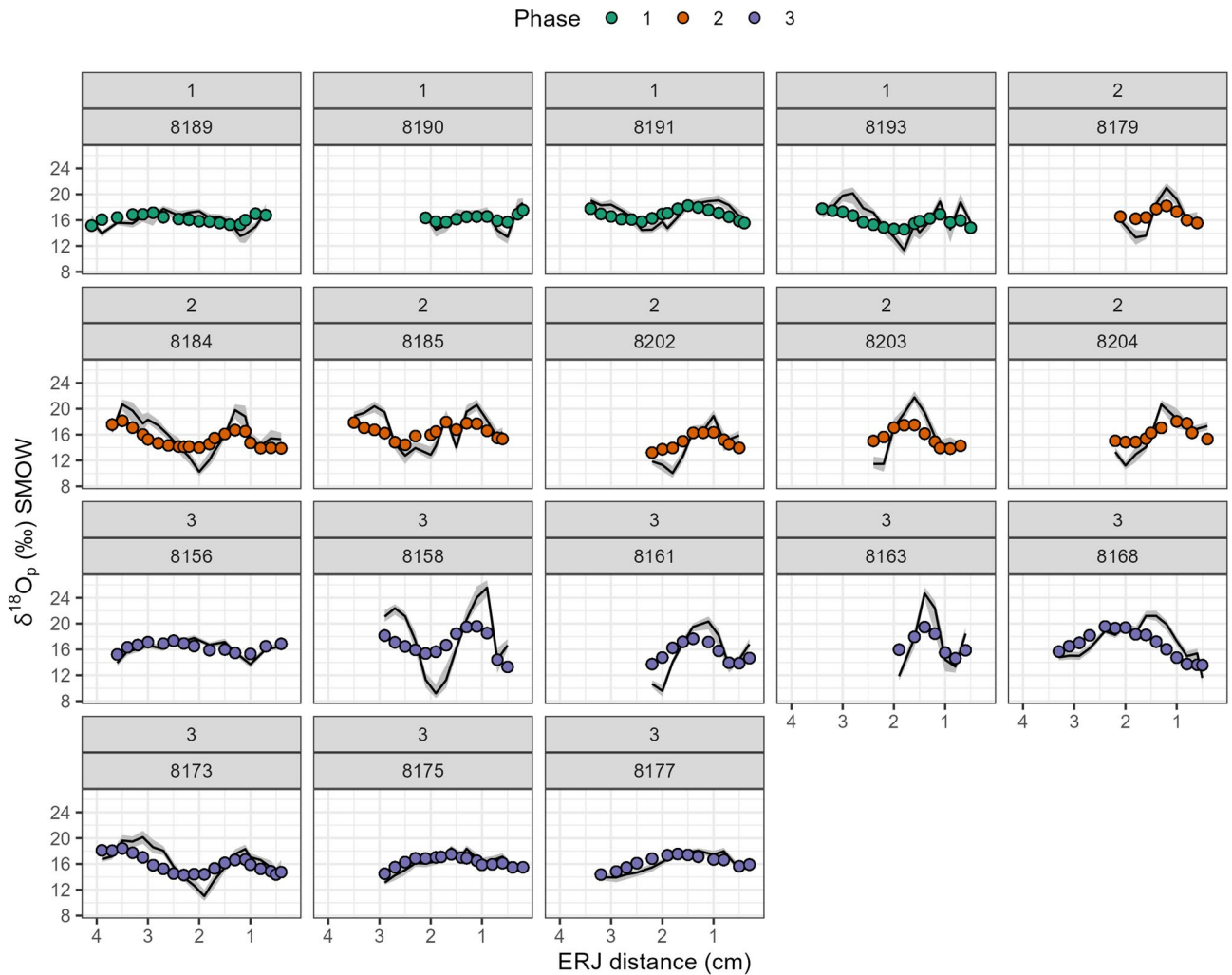


Fig. 12. Modelled input $\delta^{18}\text{O}$ profiles calculated from phosphate (‰ SMOW). Circles are the Dalmeri $\delta^{18}\text{O}$ enamel values⁷⁴ and coloured according to the occupation phase. Black lines are the input data obtained by inverse modelling⁶⁸. The gray ribbons represent the maximum and minimum estimations from the model. The distance measured from the enamel-root junction (cm) is on the x-axis.

and equipped with UV-light to minimise exogenous DNA contamination. During the analyses, strict ancient DNA authenticity criteria were followed to support the authenticity of the results^{78,79}. Sampling for the analyses was performed on the teeth: the surface of each sample was smoothly cleaned with 4% HCl, rinsed in 80% EtOH and then sterilised under UV-light for 20'. Before extraction, approximately 100 mg of dentine powder was collected in an Eppendorf tube 2 ml drilling the bone with a precision drill (Dremel 8200). To reduce friction, we used a dental bit at a low rotation rate. The samples were extracted following the procedure using a silica-based protocol⁸⁰ modified as in Fontani et al.⁸¹. Molecular concentration was initially measured on a Qubit fluorometer, and DNA extracts were used for single-stranded DNA libraries construction following the protocol of Kapp et al.⁸². The libraries were purified with the MinElute PCR purification kit (Qiagen, Hilden, Germany) and quantified using Agilent 2100 Bioanalyzer DNA 1000 chips. Eleven out of twelve libraries reported good molecular content and were pooled in equimolar amounts for shotgun sequencing on HiSeqX Ten 2 × 150 bp lane.

Bioinformatic analysis for genetic data

We processed raw genetic data using EAGER v.2.5.1⁸³. Forward (AGATCGGAAGAGCACACGTCTGAACTCCAGTCAC) and reverse adapters (AGATCGGAAGAGCGTCGTGTAGGGAAAGAGTGTGA) were trimmed, allowing filtering for clipped read length < 30, minimum read quality ~ 20 and minimum adapter overlap ~ 1. We evaluated DNA preservation by mapping reads to the *Capra hircus* genome assembly (GCA_001704415.2_ARS1.2) using the bwa *aln* algorithm, allowing for a minimum number of mismatch ~ 0.01, maximum edit distance ~ 2 and length of seeds ~ 1024. We filtered out reads with mapping quality < 30 and removed duplicates with *markduplicates*. To reduce bias in genotyping from non-UDG-treated reads, we clipped off 5 bases from left and right ends of single-stranded mapped sequences. Post mortem damage patterns were calculated using DamageProfiler, with length filter ~ 100 and number of bases for each read to be considered ~ 30. Summary

statistics were automatically generated by EAGER using multiqc, qualimap and samtools. We reconstructed two mitogenomic datasets by using EAGER v2.5.1 again to process and map newly generated and available data from the literature against the *C. hircus* mitochondrial reference genome (NC_005044.2) and the *Capra ibex* mitochondrial reference genome (NC_020623). For the ancient samples, we used the mapDamage *rescale* option to downscale base quality for those positions of the mapped files that were affected by deamination patterns. Modern samples were directly reconstructed from full-length, deduplicated .bam files, along with the samples produced in 2022 by Robin et al.⁶, which underwent UDG treatment. We used Mutect2⁸⁴ to call variants from the bam files, and bcftools⁸⁵ to normalise and filter the resulting variants by applying a minimum allele frequency (AF) > 0.5 for all samples, and minimum allele depth (AD) coverage > 3 for low coverage samples ($n = 12$) and AD > 5 for all other samples. Consensus mitogenomes for each individual were reconstructed using bcftools consensus command.

Mitochondrial DNA investigation

Phylogenetic analysis

To investigate the phylogenetic relationships of *Capra ibex* from Riparo Dalmeri, we generated three distinct mitogenome datasets: “Capra_all”, “Capra_ibex/pyrenaica”, and “Capra_ibex” (Supplementary Data 4). These datasets were constructed by combining new sequences from the six specimens obtained in this study with previously published mitogenomes of various *Capra* species, along with five sheep individuals used as an outgroup^{6,7,86,87}. Only samples with mean coverage $\geq 10x$ were retained to build the datasets. Due to the difficulty of unambiguously identifying small remains of Alpine ibex compared to other *Capra* species based on morphology, we first constructed a maximum likelihood tree using the dataset *Capra_all*, to confirm the species of our samples. The software IQTree v2.0.3 (<https://doi.org/10.1093/molbev/msaa015>) was used for the tree with the *-m TESTNEW* command to search the best-fit model (TIM2 + F + I + G4 chosen according to BIC). We performed a nonparametric bootstrap analysis with 1000 replicates and a search for the best-scoring maximum likelihood tree. Results were graphically visualised with FigTree⁸⁸ and edited in Adobe Illustrator. To validate the decision to include only samples with a coverage $\geq 10x$, the same tree was constructed using the mitogenome dataset “Capra_all_low”, with all available samples (Supplementary Fig. S8). Quality assessment of the low-coverage mitogenomes from Cogola, Romagnano and Riparo Dalmeri is provided in the Supplementary Text.

To conduct a more in-depth analysis of the relationships among the *C. ibex* samples and to estimate the divergence times between Alpine ibex and Iberian ibex, we performed Bayesian inference using the “Capra_ibex/pyrenaica” dataset. We ran the analysis with the software BEAST v2.7.1⁸⁹ and the BEAST package bdsky v1.4.5⁹⁰. Default parameters were used except for the root node, which was set to 20,000 years as the starting point for the birth-death skyline serial prior (the root node must be older than the oldest sample, which is 13400 cal. BP in this case). The package BEAST Model Test⁹¹ was used to find the best substitution model, and mutation rate estimation was performed under a strict clock assumption. A Markov Chain Monte Carlo (MCMC) run with 2.5×10^7 generations was conducted, sampling every 1,000 steps. The chain convergence and effective sampling size (ESS) values were evaluated using Tracer v1.7.2⁹². The first 10% trees were discarded as a burn-in, and the Maximum Clade Credibility tree was obtained using TreeAnnotator v2.7.1. Results were graphically visualised with FigTree⁸⁸ and edited in Adobe Illustrator.

Haplotype diversity among the Alpine ibex from Riparo Dalmeri was explored building a TCS network from the dataset “Capra_ibex”. The network was constructed using PopArt⁹³. We used the incorporated TCS algorithm, which calculates an absolute pairwise distance matrix of all haplotypes and connects them on the basis of the parsimony criterion to minimise mutation steps between haplotypes. The resulting network was refined in Adobe Illustrator.

Genetic distance and mitochondrial diversity

To better explain the Network results, using the dataset “Capra_ibex”, we calculated the average pairwise distances for all ancient, historic and modern samples of *Capra ibex*, assuming they belong to distinct lineages. Also, we categorised the samples from the same dataset into five groups based on mitochondrial haplogroups and computed the within-groups mean distances for them to compare the genetic diversity for the different populations within *C. ibex* (Supplementary Table S4). Distance calculations were conducted using MEGA X⁹⁴, with gaps and missing data handled as pairwise deletions to preserve the maximum number of homologous sequences. To analyse the mitochondrial genetic diversity, we used the dataset “Capra_ibex”. First, we divided the sequences in four age-sample groups: Dalmeri (13500 cal. BP to 11500 cal. BP), ancient (9700 cal. BP to 3500 cal. BP), historic (950 cal. BP to 1919 CE), and modern individuals. Subsequently, for each group, we calculated the number of haplotypes (Nh), haplotype diversity (h), segregation sites (S) and nucleotide diversity (π) with the R v4.4.0 software packages Pegas v1.3⁹⁵ (Supplementary Table S5).

Demographic analyses

To infer the changes in population history of Alpine ibex over the last 30000 years, we used a Bayesian Skyline coalescent prior applied to the mitogenomes⁹⁴. To obtain the skyline plot, we used the dataset “Capra_ibex” and performed the analysis with Beast v2.7.1⁸⁹. The package BEAST Model Test⁹¹ was used to estimate the best substitution model, with a mutation rate of $2.73e^{-796,97.1}$ under a stick clock. We ran a MCMC chain of 2.5×10^7 samples and visualised the MCMC chain convergence using Tracer v1.7.2⁹².

Genetic sex determination

We used EAGER with the same parameters listed above to map shotgun sequences to the reference genome sequence of the Saanen domestic goat (GCA_015443085.1), the only available *Capra hircus* genome at the time of writing, which presented annotated sex chromosomes. We tested sex assignment using the so-called “Mittnik

approach⁹⁸, modified according to De Flamingh et al.⁹⁹ (see here: <https://www.ncbi.nlm.nih.gov/pmc/articles/PMC7144076/>). We combined the “Skoglund approach”¹⁰⁰ with the approach presented in Denoyelle et al.¹⁰¹ to validate our results. Detailed explanation can be found in Supplementary Tables S6, S7 and S8.

Data availability

Raw sequencing data are publicly available in the European Nucleotide Archive under project number PR-JEB87623 (data is private pending evaluation). All the proteomic raw data, the MaxQuant evidence file, and the deamidation R script were uploaded to Zenodo (<https://doi.org/10.5281/zenodo.15024003>). Isotope data are available within the manuscript and its supplementary material. The OxCal code used for modelling the radio-carbon dates of Riparo Dalmeri was uploaded to Zenodo (<https://doi.org/10.5281/zenodo.15063853>).

Received: 20 May 2025; Accepted: 10 December 2025

Published online: 27 February 2026

References

- Parrini, F., Cain, J. W. & Krausman, P. R. *Capra Ibex* (Artiodactyla: Bovidae). *Mammalian Species*. **830**, 1–12 (2009).
- Stüwe, M. & Nievergelt, B. Recovery of Alpine ibex from near extinction: The result of effective protection, captive breeding, and reintroductions. *Appl. Anim. Behav. Sci.* **29**, 379–387 (1991).
- Toïgo, C., Brambilla, A., Grignolio, S. & Pedrotti, L. The IUCN Red List of Threatened Species 2020: e.T42397A161916377. <https://doi.org/10.2305/IUCN.UK.2020-2.RLTS.T42397A161916377.en>.
- Semenzato, P. et al. Behavioural heat-stress compensation in a cold-adapted ungulate: Forage-mediated responses to warming alpine summers. *Ecol. Lett.* **24**, 1556–1568 (2021).
- Brivio, F. et al. Forecasting the response to global warming in a heat-sensitive species. *Sci. Rep.* **9**, 3048 (2019).
- Robin, M. et al. Ancient mitochondrial and modern whole genomes unravel massive genetic diversity loss during near extinction of Alpine ibex. *Mol. Ecol.* **31**, 3548–3565 (2022).
- Grossen, C., Guillaume, F., Keller, L. F. & Croll, D. Purging of highly deleterious mutations through severe bottlenecks in Alpine ibex. *Nat. Commun.* **11**, 1001 (2020).
- Fiore, I. & Tagliacozzo, A. Lo sfruttamento delle risorse animali nei siti di altura e di fondovalle nel Tardiglaciale dell’Italia nord-orientale. in *Pleistocene Alpina* (eds Malerba, G. & Visintini, P.) 97–109 (2005).
- Bertola, S. et al. L’Epigravettiano recente nell’area prealpina e alpina orientale. in *L’Italia Tra 15.000 E 10.000 anni fa: Cosmopolitismo e regionalità nel Tardoglaciale* (ed Martini, F.). Museo fiorentino di preistoria Paolo Graziosi, Firenze (2007).
- Tagliacozzo, A. & Fiore, I. Hunting strategies in a mountain environment during the late glacial in North Eastern Italy. *Pleistocene Alpina*. **44**, 79–93 (2009).
- Dalmeri, G. et al. Riparo Dalmeri: Le pietre dipinte dell’area rituale. *Pleistocene Alpina*. **45**, 67–117 (2011).
- Angelucci, D. E. et al. La successione esterna del Riparo Dalmeri (Trento, Italia). Prime informazioni geoarcheologiche. *Pleistocene Alpina*. **45**, 127–146 (2011).
- Ravazzi, C. An overview of the Quaternary continental stratigraphic units based on biological and climatic events in Italy. *J. Quat. Sci.* **16**, 11–18 (2003).
- Dalmeri, G. et al. The ochre painted stones from the Riparo dalmeri (Trento). Development of the research on the art and rituality of the Epigravettian site. *Pleistocene Alpina*. **44**, 95–119 (2009).
- Phoca-Cosmetatou, N. Specialisation & diversification: A Tale of two subsistence strategies from late glacial Italy. *Before Farming*. **3**, 1–29 (2009).
- Lugli, F. et al. A strontium isoscape of Italy for provenance studies. *Chem. Geol.* **587**, 120624 (2022).
- Lehner, B. & Grill, G. Global river hydrography and network routing: Baseline data and new approaches to study the world’s large river systems. *Hydrol. Process.* **27**, 2171–2186 (2013).
- Hartmann, J. & Moosdorf, N. The new global lithological map database glim: A representation of rock properties at the Earth surface. *Geochem. Geophys. Geosyst.* **13**, 2012GC004370 (2012).
- Kohn, M. J. Carbon isotope compositions of terrestrial C3 plants as indicators of (paleo)ecology and (paleo)climate. *Proc. Natl. Acad. Sci. U.S.A.* **107**, 19691–19695 (2010).
- Still, C. J., Berry, J. A., Collatz, G. J. & DeFries, R. S. Global distribution of C₃ and C₄ vegetation: Carbon cycle implications. *Global Biogeochem. Cycles* **17**, (2003).
- Pederzani, S. & Britton, K. Oxygen isotopes in bioarchaeology: Principles and applications, challenges and opportunities. *Earth-Sci. Rev.* **188**, 77–107 (2019).
- Nelson, D. B., Basler, D. & Kahmen, A. Precipitation isotope time series predictions from machine learning applied in Europe. *Proc. Natl. Acad. Sci. U.S.A.* **118**, e2024107118 (2021).
- Couturier, M. A. Le bouquetin des Alpes: *Capra Aegagrus Ibex* L. Grenoble (1962).
- Fiore, I., Tagliacozzo, A. & Cassoli, P. F. Ibex exploitation at Dalmeri rockshelter (TN) and specialized hunting in the sites of the Eastern Alps during the Tardiglacial and the Early Holocene. *Pleistocene Alpina*. **34**, 173–183 (2001).
- Villa, G. & Giacobini, G. Nuovi denti umani dai livelli epigravettiani di Riparo Dalmeri (TN). *Pleistocene Alpina*. **41**, 245–250 (2005).
- Alciati, G. et al. Human deciduous dental crowns from the epigravettian layers at Riparo Dalmeri (Trento). A preliminary descriptive note. *Pleistocene Alpina*. **34**, 197–200 (2001).
- Fiore, I. & Tagliacozzo, A. Lo Sfruttamento Dello Stambecco nel tardiglaciale Di Riparo dalmeri (TN): Il Livello 26c. in *Archaeozoological Studies in Honour of Alfredo Riedel* (Bolzano, 2006).
- Seguinot, J. et al. Modelling last glacial cycle ice dynamics in the Alps. *Cryosphere* **12**, 3265–3285 (2018).
- Boxleitner, M. et al. Late Pleistocene – Holocene surface processes and landscape evolution in the central Swiss Alps. *Geomorphology* **295**, 306–322 (2017).
- Brambilla, A., Von Hardenberg, A., Nelli, L. & Bassano, B. Distribution, status, and recent population dynamics of Alpine ibex *Capra Ibex* in Europe. *Mamm. Rev.* **50**, 267–277 (2020).
- Curci, A. & Tagliacozzo, A. Determinazione dell’età di morte e della stagione di cattura attraverso lo studio dei livelli di accrescimento di cemento e dentina nei denti di mammiferi: L’esempio Di Riparo Dalmeri (TN). in *Atti Del 2° Convegno Nazionale Di Archeozoologia* (Asti, 1997), ABACO Edizioni, Forlì, (2000).
- Chauveau, V. et al. Identifying the environmental drivers of corridors and predicting connectivity between seasonal ranges in multiple populations of Alpine ibex (*Capra Ibex*) as tools for conserving migration. *Divers. Distrib.* **30**, e13894 (2024).
- Parrini, F., Grignolio, S., Luccarini, S., Bassano, B. & Apollonio, M. Spatial behaviour of adult male Alpine ibex *Capra Ibex* in the Gran Paradiso National Park, Italy. *Acta Theriol.* **48**, 411–423 (2003).
- Herfindal, I., Anderwald, P., Filli, E., Campell Andri, S. & Rempfler, T. Climate, competition and weather conditions drive vertical displacement and habitat use of an alpine ungulate in a highly topographic landscape. *Landsc. Ecol.* **34**, 2523–2539 (2019).

35. Grignolio, S., Rossi, I., Bassano, B. & Apollonio, M. Predation risk as a factor affecting sexual segregation in Alpine ibex. *J. Mammal.* **88**, 1488–1497 (2007).
36. Grignolio, S., Rossi, I., Bassano, B., Parrini, F. & Apollonio, M. Seasonal variations of spatial behaviour in female alpine ibex (*Capra Ibex Ibex*) in relation to Climatic conditions and age. *Ethol. Ecol. Evol.* **16**, 255–264 (2004).
37. Cerling, T. E. & Harris, J. M. Carbon isotope fractionation between diet and bioapatite in ungulate mammals and implications for ecological and paleoecological studies. *Oecologia* **120**, 347–363 (1999).
38. Manzella, G. et al. Paleoecology of mid-mountain Alps (Trentino, Italy) between Greenland interstadial 1 and Early Holocene. Carbon and nitrogen stable isotope analysis of ibex and red deer. *Q. Sci. Rev.* **328**, 108549 (2024).
39. Lazzarini, N. et al. The isotope record ($\delta^{13}\text{C}$, $\delta^{18}\text{O}$) of vertical mobility in incremental tissues (tooth enamel, hair) of modern livestock: A reference set from the Mongolian Altai. *Quat Int.* **595**, 128–144 (2021).
40. Heaton, T. H. E. Spatial, species, and Temporal variations in the $^{13}\text{C}/^{12}\text{C}$ ratios of C_3 plants: Implications for Palaeodiet studies. *J. Archaeol. Sci.* **26**, 637–649 (1999).
41. Körner, C., Farquhar, G. D. & Roksandic, Z. A global survey of carbon isotope discrimination in plants from high altitude. *Oecologia* **74**, 623–632 (1988).
42. Makarewicz, C. A., Arbuckle, B. S. & Öztan, A. Vertical transhumance of sheep and goats identified by intra-tooth sequential carbon ($\delta^{13}\text{C}$) and oxygen ($\delta^{18}\text{O}$) isotopic analyses: Evidence from chalcolithic Köşk Höyük, central Turkey. *J. Archaeol. Sci.* **86**, 68–80 (2017).
43. Tornero, C. et al. The altitudinal mobility of wild sheep at the epigravettian site of Kalavan 1 (Lesser Caucasus, Armenia): Evidence from a sequential isotopic analysis in tooth enamel. *J. Hum. Evol.* **97**, 27–36 (2016).
44. Brambilla, A. et al. Dietary differences in males and females of a strongly sexually dimorphic ungulate. *Eur. J. Wildl. Res.* **70**, 98 (2024).
45. Tichon, J. et al. Population dynamics and the effect of drought in the threatened Nubian ibex. *Wildl. Soc. Bull.* **47**, e1397 (2023).
46. Makarewicz, C. A. & Pederzani, S. Oxygen ($\delta^{18}\text{O}$) and carbon ($\delta^{13}\text{C}$) isotopic distinction in sequentially sampled tooth enamel of co-localized wild and domesticated caprines: Complications to Establishing seasonality and mobility in herbivores. *Palaeogeogr Palaeoclimatol Palaeoecol.* **485**, 1–15 (2017).
47. Schenk, F. et al. Warm summers during the Younger Dryas cold reversal. *Nat. Commun.* **9**, 1634 (2018).
48. Bromley, G. R. M. et al. Younger Dryas deglaciation of Scotland driven by warming summers. *Proc. Natl. Acad. Sci. U.S.A.* **111**, 6215–6219 (2014).
49. Mussi, M. & Peresani, M. Human settlement of Italy during the Younger Dryas. *Quat Int.* **242**, 360–370 (2011).
50. Brivio, F. et al. Seeking temporal refugia to heat stress: Increasing nocturnal activity despite predation risk. *Proc. R Soc. B.* **291**, 20231587 (2024).
51. Bökönyi, S. A new method for the determination of the number of individuals in animal bone material. *Am. J. Archaeol.* **74**, 291–292 (1970).
52. Holt, E., Evans, J. A. & Madgwick, R. Strontium ($^{87}\text{Sr}/^{86}\text{Sr}$) mapping: A critical review of methods and approaches. *Earth Sci. Rev.* **216**, 103593 (2021).
53. Longin, R. New method of collagen extraction for radiocarbon dating. *Nature* **230**, 241–242 (1971).
54. D'Elia, M. et al. Sample Preparation and blank values at the AMS radiocarbon facility of the university of Lecce. *Nucl. Instrum. Methods Phys. Res. B.* **223–224**, 278–283 (2004).
55. Calcagnile, L., Quarta, G. & D'Elia, M. High-resolution accelerator-based mass spectrometry: Precision, accuracy and background. *Appl. Radiat. Isot.* **62**, 623–629 (2005).
56. Stuiver, M. & Polach, H. A. Discussion reporting of ^{14}C data. *Radiocarbon* **19**, 355–363 (1977).
57. Reimer, P. J. et al. The IntCal20 Northern hemisphere radiocarbon age calibration curve (0–55 cal kBP). *Radiocarbon* **62**, 725–757 (2020).
58. Bronk Ramsey, C. Bayesian analysis of radiocarbon dates. *Radiocarbon* **51**, 337–360 (2009).
59. Bronk Ramsey, C. Dealing with outliers and offsets in radiocarbon dating. *Radiocarbon* **51**, 1023–1045 (2009).
60. Ramsey, B. OxCal v.4.4.4. (2021).
61. Argentino, C., Lugli, F., Cipriani, A. & Panieri, G. Testing miniaturized extraction chromatography protocols for combined $^{87}\text{Sr}/^{86}\text{Sr}$ and $\delta^{88}/^{86}\text{Sr}$ analyses of pore water by MC-ICP-MS. *Limnol. Oceanography: Methods.* **19**, 431–440 (2021).
62. Lugli, F., Cipriani, A., Tavaglione, V., Traversari, M. & Benazzi, S. Transhumance pastoralism of Roccapelago (Modena, Italy) early-modern individuals: Inferences from Sr isotopes of hair strands. *Am. J. Phys. Anthropol.* **167**, 470–483 (2018).
63. Lugli, F., Cipriani, A., Peretto, C., Mazzucchelli, M. & Brunelli, D. In situ high spatial resolution $^{87}\text{Sr}/^{86}\text{Sr}$ ratio determination of two Middle Pleistocene (c.a. 580 ka) *Stephanorhinus hundsheimensis* teeth by LA-MC-ICP-MS. *Int. J. Mass Spectrom.* **412**, 38–48 (2017).
64. Berglund, M. & Wieser, M. E. Isotopic compositions of the elements 2009 (IUPAC Technical Report). *Pure Appl. Chem.* **83**, 397–410 (2011).
65. McArthur, J. M., Howarth, R. J. & Bailey, T. R. Strontium isotope stratigraphy: LOWESS version 3: Best fit to the marine Sr isotope curve for 0–509 Ma and accompanying look-up table for deriving numerical age. *J. Geol.* **109**, 155–170 (2001).
66. Vonhof, H. B. et al. High-precision stable isotope analysis of $< 5 \mu\text{g CaCO}_3$ samples by continuous-flow mass spectrometry. *Rapid Comm. Mass Spectrom.* **34**, e8878 (2020).
67. Passey, B. H. et al. Inverse methods for estimating primary input signals from time-averaged isotope profiles. *Geochim. Cosmochim. Acta.* **69**, 4101–4116 (2005).
68. Passey, B. H. & Cerling, T. E. Tooth enamel mineralization in ungulates: Implications for recovering a primary isotopic time-series. *Geochim. Cosmochim. Acta.* **66**, 3225–3234 (2002).
69. Kohn, M. J., Comment, B. H., Passey & Cerling, T. E. *Geochim. Cosmochim. Acta.* **68**, 403–405 (2004). (2002).
70. Pederzani, S. et al. Stable isotopes show homo sapiens dispersed into cold steppes ~45,000 years ago at Ilsenhöhle in Ranis, Germany. *Nat. Ecol. Evol.* **8**, 578–588 (2024).
71. Pederzani, S. et al. Subarctic climate for the earliest *Homo sapiens* in Europe. *Sci. Adv.* **7**, eabi4642 (2021).
72. Zazzo, A. et al. The isotope record of short- and long-term dietary changes in sheep tooth enamel: Implications for quantitative reconstruction of paleodiets. *Geochim. Cosmochim. Acta.* **74**, 3571–3586 (2010).
73. Iacumin, P., Bocherens, H., Mariotti, A. & Longinelli, A. Oxygen isotope analyses of co-existing carbonate and phosphate in biogenic apatite: A way to monitor diagenetic alteration of bone phosphate? *EPSL* **142**, 1–6 (1996).
74. Delgado-Huertas, A., Iacumin, P., Stenni, B., Sánchez Chillón, B. & Longinelli, A. Oxygen isotope variations of phosphate in mammalian bone and tooth enamel. *Geochim. Cosmochim. Acta.* **59**, 4299–4305 (1995).
75. Pryor, A. J. E., Stevens, R. E., O'Connell, T. C. & Lister, J. R. Quantification and propagation of errors when converting vertebrate biomineral oxygen isotope data to temperature for palaeoclimate reconstruction. *Palaeogeogr Palaeoclimatol Palaeoecol.* **412**, 99–107 (2014).
76. Cappellini, E. et al. Early Pleistocene enamel proteome from Dmanisi resolves *Stephanorhinus* phylogeny. *Nature* **574**, 103–107 (2019).
77. Lugli, F. et al. Enamel peptides reveal the sex of the late antique 'Lovers of Modena'. *Sci. Rep.* **9**, 13130 (2019).
78. Knapp, M., Clarke, A. C. & Horsburgh, K. A. Matisoo-Smith, E. A. Setting the stage – Building and working in an ancient DNA laboratory. *Ann. Anat.* **194**, 3–6 (2012).

79. Llamas, B. et al. From the field to the laboratory: Controlling DNA contamination in human ancient DNA research in the high-throughput sequencing era. *STAR* **3**, 1–14 (2017).
80. Dabney, J. et al. Complete mitochondrial genome sequence of a Middle Pleistocene cave bear reconstructed from ultrashort DNA fragments. *Proc. Natl. Acad. Sci. U S A.* **110**, 15758–15763 (2013).
81. Fontani, F. et al. Bioarchaeological and paleogenomic profiling of the unusual neolithic burial from Grotta Di Pietra Sant'Angelo (Calabria, Italy). *Sci. Rep.* **13**, 11978 (2023).
82. Kapp, J. D., Green, R. E. & Shapiro, B. A fast and efficient single-stranded genomic library preparation method optimized for ancient DNA. *J. Hered.* **112**, 241–249 (2021).
83. Fellows Yates, J. A. et al. Reproducible, portable, and efficient ancient genome reconstruction with nf-core/eager. *PeerJ* **9**, e10947 (2021).
84. Cibulskis, K. et al. Sensitive detection of somatic point mutations in impure and heterogeneous cancer samples. *Nat. Biotechnol.* **31**, 213–219 (2013).
85. Danecek, P. et al. Twelve years of samtools and BCFtools. *GigaScience* **10**, giab008 (2021).
86. Alberto, F. J. et al. Convergent genomic signatures of domestication in sheep and goats. *Nat. Commun.* **9**, 813 (2018).
87. Maixner, F. et al. The Iceman's last meal consisted of fat, wild meat, and cereals. *Curr. Biol.* **28**, 2348–2355e9 (2018).
88. Rambaut, A. FigTree v1.4.3. (2012). Available from <http://tree.bio.ed.ac.uk/software/figtree/>
89. Bouckaert, R. et al. BEAST 2: A software platform for bayesian evolutionary analysis. *PLoS Comput. Biol.* **10**, e1003537 (2014).
90. Stadler, T., Kühnert, D., Bonhoeffer, S. & Drummond, A. J. Birth–death skyline plot reveals temporal changes of epidemic spread in HIV and hepatitis C virus (HCV). *Proc. Natl. Acad. Sci. U.S.A.* **110**, 228–233 (2013).
91. Bouckaert, R. R., Drummond, A. J. & bModelTest Bayesian phylogenetic site model averaging and model comparison. *BMC Evol. Biol.* **17**, 42 (2017).
92. Rambaut, A., Drummond, A. J., Xie, D., Baele, G. & Suchard, M. A. Posterior summarization in bayesian phylogenetics using tracer 1.7. *Syst. Biol.* **67**, 901–904 (2018).
93. Leigh, J. W. & Bryant, D. Popart: Full-feature software for haplotype network construction. *Methods Ecol. Evol.* **6**, 1110–1116 (2015).
94. Stecher, G., Tamura, K. & Kumar, S. Molecular evolutionary genetics analysis (MEGA) for MacOS. *Mol. Biol. Evol.* **37**, 1237–1239 (2020).
95. Paradis, E. Pegas: an R package for population genetics with an integrated–modular approach. *Bioinformatics* **26**, 419–420 (2010).
96. Nomura, K. et al. Domestication process of the goat revealed by an analysis of the nearly complete mitochondrial protein-encoding genes. *PLoS ONE.* **8**, e67775 (2013).
97. Tarekegn, G. M. et al. Mitochondrial DNA variation reveals maternal origins and demographic dynamics of Ethiopian indigenous goats. *Ecol. Evol.* **8**, 1543–1553 (2018).
98. Mittnik, A., Wang, C. C., Svoboda, J. & Krause, J. A molecular approach to the sexing of the triple burial at the upper paleolithic site of Dolní Věstonice. *PLoS ONE.* **11**, e0163019 (2016).
99. De Flamingh, A., Coutu, A., Roca, A. L. & Malhi, R. S. Accurate sex identification of ancient elephant and other animal remains using low-coverage DNA shotgun sequencing data. *G3 (Bethesda).* **10**, 1427–1432 (2020).
100. Skoglund, P., Storå, J., Götherström, A. & Jakobsson, M. Accurate sex identification of ancient human remains using DNA shotgun sequencing. *J. Archaeol. Sci.* **40**, 4477–4482 (2013).
101. Denoyelle, L. et al. VarGoats project: A dataset of 1159 whole-genome sequences to dissect *Capra Hircus* global diversity. *Genet. Sel. Evol.* **53**, 86 (2021).

Acknowledgements

We thank the Soprintendenza per i Beni Culturali of the Autonomous Province of Trento, and the MUSE - Science Museum of Trento for granting access to the archaeological materials analysed in this study. Dr. Diego Pinetti and Dr. Filippo Genovese of the Centro Interdipartimentale Grandi Strumenti (UNIMORE) are acknowledged for technical assistance during LC-MS/MS analyses. We also thank Prof. Luca Pagani (University of Padua) for his feedback and comments, which have provided helpful insights for this work. Nerobutto sponsored research activities on prehistory carried out at Muse - Science Museum of Trento between 2019 and 2025. F.L. is supported by the European Union's Horizon Europe Research and Innovation programme under the Marie Skłodowska-Curie Actions PF (grant agreement no. 101104566—AROUSE). M.R. is supported by CHANGE-S, SPOKE 5 “Science and Technologies for Sustainable Diagnostics of Cultural Heritage”, PE 0000020, CUP B53C22003890006, NRP M4C2, Investment 1.3, funded by the European Union—NextGenerationEU. S.S. is supported by the ERC FIRSTSTEPS project (Grant Agreement ID: 101019659). Open access publication was funded by the Department of Cultural Heritage through a grant awarded to F.F. and by the European Research Council (ERC) under the European Union's Horizon 2020 research and innovation programme (grant agreement No 724046- SUCCESS, PI: S.B).

Author contributions

M.R., E.B., S.B., F.L. and A.C. designed the research; M.R., G.D., A.F., N.N. and R.D. conducted fieldwork and sample collection; E.A., F.F., R.I., E.C., A.L., F.L., G.T., S.S., H.V., L.C. and G.Q. performed the experiments and collected data; E.A., F.F., R.I., F.L., A.C., M.R., E.B., L.C. and G.Q. analysed the data and interpreted the results; E.A. and F.F. wrote the manuscript with contributions from all authors; A.C., F.L., M.R. and E.B. revised and edited the manuscript; M.R. supervised the project and provided guidance; M.R., A.C., S.B. and D.L. coordinated research activities and ensured project completion; M.R., S.B., A.C. and F.L. secured funding and managed financial resources.

Declarations

Competing interests

The authors declare no competing interests.

Additional information

Supplementary Information The online version contains supplementary material available at <https://doi.org/10.1038/s41598-025-32389-w>.

Correspondence and requests for materials should be addressed to E.A., F.F. or M.R.

Reprints and permissions information is available at www.nature.com/reprints.

Publisher's note Springer Nature remains neutral with regard to jurisdictional claims in published maps and institutional affiliations.

Open Access This article is licensed under a Creative Commons Attribution 4.0 International License, which permits use, sharing, adaptation, distribution and reproduction in any medium or format, as long as you give appropriate credit to the original author(s) and the source, provide a link to the Creative Commons licence, and indicate if changes were made. The images or other third party material in this article are included in the article's Creative Commons licence, unless indicated otherwise in a credit line to the material. If material is not included in the article's Creative Commons licence and your intended use is not permitted by statutory regulation or exceeds the permitted use, you will need to obtain permission directly from the copyright holder. To view a copy of this licence, visit <http://creativecommons.org/licenses/by/4.0/>.

© The Author(s) 2026